RAMBOLL

ENVIRONMENT
& HEALTH

MEMORANDUM

Job	**SATES Phase IA Part 2 Initial Test Plot Characterization Mineralogy Data Transmittal**
Client	**Teck American Incorporated**
Date	**July 19, 2018**
To	**Dave Enos and Denise Mills**
From	**Amy Kephart**
Copy to	**Kris McCaig, Teck American Incorporated; Cristy Kessel, Teck American Incorporated; Mike Arnold, Ramboll; Rosalind Schoof, Ramboll**

1. Introduction

Upper Columbia River (UCR) Soil Amendment Technology Evaluation Study (SATES) test plot characterization was conducted in accordance with the *Final Work Plan for the Soil Amendment Technology Evaluation Study (SATES), Phase I: Test Plot Characterization and Initial Amendment Alternatives Evaluation* (Work Plan; Ramboll 2017a) and Addendum (Ramboll 2017b). Test plots 401-1, 401-2, 441-2, 258-3 were selected for further analysis in this characterization phase.

Samples collected at the location of the highest soil lead concentration on each of the four test plots were submitted for soil mineralogical analysis. Analysis was conducted using X-ray absorption spectroscopy by the United States Environmental Protection Agency (EPA) and QEMSCAN by Hazen Research, Inc. (Hazen).

A summary of the findings by EPA (see Attachment A) and Hazen (see Attachment B) are included as attachments to this memo.

In Attachment A, EPA's results are presented using laboratory sample identification numbers. A summary table linking the EPA laboratory identification numbers to the SATES Phase IA Part 2 soil sample identification numbers is included below to facilitate review with other SATES Phase IA Part 2 results.

Ramboll
901 Fifth Avenue
Suite 2820
Seattle, WA 98164
USA

T +1 206 336 1650
F +1 206 336 1651
www.ramboll.com

SATES Phase IA Part 2 Sample ID	EPA Lab ID
IC-401-1A-101017	Pb_K17_001
IC-401-1B-101017	Pb_K17_002
IC-401-1C-101117	Pb_K17_003
IC-401-1C-101117-D	Pb_K17_004
IC-401-1D-101117	Pb_K17_005
IC-401-2B-101117	Pb_K17_006
IC1-401-2A-101217	Pb_K17_007
IC2-401-2A-101217	Pb_K17_008
IC3-401-2A-101217	Pb_K17_009
IC-401-2C-101217	Pb_K17_010
IC-401-2D-101217	Pb_K17_011
IC-258-3A-101717	Pb_K17_012
IC-258-3B-101717	Pb_K17_013
IC-258-3C-101717	Pb_K17_014
IC-258-3D-101717	Pb_K17_015
IC-441-1A-101617	Pb_K17_016
IC-441-1B-101617	Pb_K17_017
IC-441-1C-101617	Pb_K17_018
IC-441-1D-101617	Pb_K17_019
D-401-1B-100317-0-3	Pb_K17_001_CDA_OUT
D-401-2C-100317-0-3	Pb_K17_002_CDA_OUT
D-258-3C-100317-0-3	Pb_K17_003_CDA_OUT
D-441-1B-100317-0-3	Pb_K17_004_CDA_OUT

2. References

Ramboll Environ U.S. Corporation (Ramboll). 2017a. FINAL Work Plan for the Soil Amendment Technology Evaluation Study Phase I: Test Plot Characterization and Initial Amendment Alternatives Evaluation. Prepared for Teck American Incorporated. Seattle, WA.

Ramboll Environ U.S. Corporation (Ramboll). 2017b. Addendum - Soil Amendment Technology Evaluation Study (SATES) Final Work Plan for the Soil Amendment Technology Evaluation Study, Phase I: Test Plot Characterization and Initial Amendment Alternatives Evaluation. Prepared for Teck American Incorporated. Seattle, WA. September 29.

RAMBOLL

ATTACHMENT A:
UCR SOIL-PB SPECIATION REPORT
EPA

Background

EPA's National Risk Management Research Laboratory (NRMRL) (Cincinnati, OH) received 23 soil samples in support of the Region 10 treatability study at the Upper Columbia River Area with coordinated efforts with the Confederated Tribes of the Colville Reservation. NRMRL's in-kind contribution to the study was to provide X-ray absorption spectroscopy analysis of the soil samples to determine the speciation of Pb in the samples prior to soil amendment and anticipate analysis of samples post treatment to determine if changes in Pb speciation are evident. Below is a brief description of X-ray absorption spectroscopy, a highlight of the methods employed, and a discussion of results for the submitted soil samples.

In the context of conducting research to understand the role that metal contaminants play in bioavailability and resulting remediation to eliminate biological availability, there are many tools available to decipher pieces of the total puzzle. Soil samples taken to the laboratory can undergo an array of analyses including batch reactors to examine kinetics and thermodynamics; chemical extractions to determine total metal content, operationally defined speciation (sequential extractions), or bioaccessibility (to mimic human bioavailability); and instrument analysis to identify mineralogy and other fundamental properties of the sample. It is at this point where most evaluations are completed and it is determined that characteristics such as metal concentration, soil pH, iron oxide concentration, and soil organic matter are indicative of the dose-response paradigm. However, aside from knowing the total metal concentration, little is often known or determined with regard to the chemistry of the metal. This information is often inferred from the soil properties – which can be a valid approach – but often involves inconclusive guesswork through the use of sequential extraction procedures or broad based modeling efforts. To gain a more complete picture of the chemistry of metals, one must employ techniques that definitively determine the speciation

(the true chemical form and physical coordination) of contaminants. There are several excellent spectroscopic methods capable of determining metal speciation but the most authoritative approach involves the application of synchrotron methods such as X-ray absorption spectroscopy (XAS). X-ray absorption spectroscopy distinguishes the oxidation state, coordination environment, interatomic bond distances, and identity of nearest-neighboring elements relative to a specific metal of concern. Information gleamed from XAS experiments provides an in-situ look at the current chemical form of a metal and can be used to predict the long-term fate of the metal and its potential bioavailability based on known solubility products. The impact of metal speciation on risk assessment has gained much attention over the past couple decades and will continue to grow in acceptance as an important part in our understanding of metal bioavailability and remediation.

X-ray absorption spectroscopy (XAS) refers to the interaction of how X-rays are absorbed by an atom at energies near and above the core-level binding energies of that particular atom. XAS is the modulation of an atom's X-ray absorption probability due to the chemical and physical state of the atom. XAS spectra are especially sensitive to the formal oxidation state, coordination chemistry, and the interatomic distances, coordination number and species of the atoms in the surrounding proximity of the selected element of interest. As a result, XAS provides a practical and simple way to determine the chemical state and local atomic structure for a selected atomic species. XAS can be used in a wide variety of systems and bulk physical environments. Since XAS is an atomic probe, nearly all substances can be studied. All elements have core shell electrons. Crystallinity is not a factor for XAS measurements making analysis of non-crystalline material, disordered compounds, and solutions feasible and attractive. XAS is capable of detection sensitivities of a few parts per million. An important aspect from an environmental perspective is that XAS is an in-situ spectroscopy allowing for the investigation of samples in their natural state.

A typical XAS spectra is broken into 2 regimes (Figure 1):

XANES - X-ray Absorption Near-Edge Spectroscopy

EXAFS - Extended X-ray Absorption Fine-Structure

which contain related, but slightly different information about an element's local coordination and chemical state. X-rays are absorbed by all matter through the photoelectric effect: An x-ray is absorbed by an atom, promoting a core-level electron (K, L, or M shell) out of the atom and into a continuum. The atom is left in an excited state with an empty electronic level (a core hole). The electron ejected from the atom is called the photoelectron. When X-rays are absorbed by the photoelectric effect, the excited core-hole will relax back to a "ground state" of the atom. A higher level core electron drops into the core hole, and a fluorescent X-ray or Auger electron is emitted.

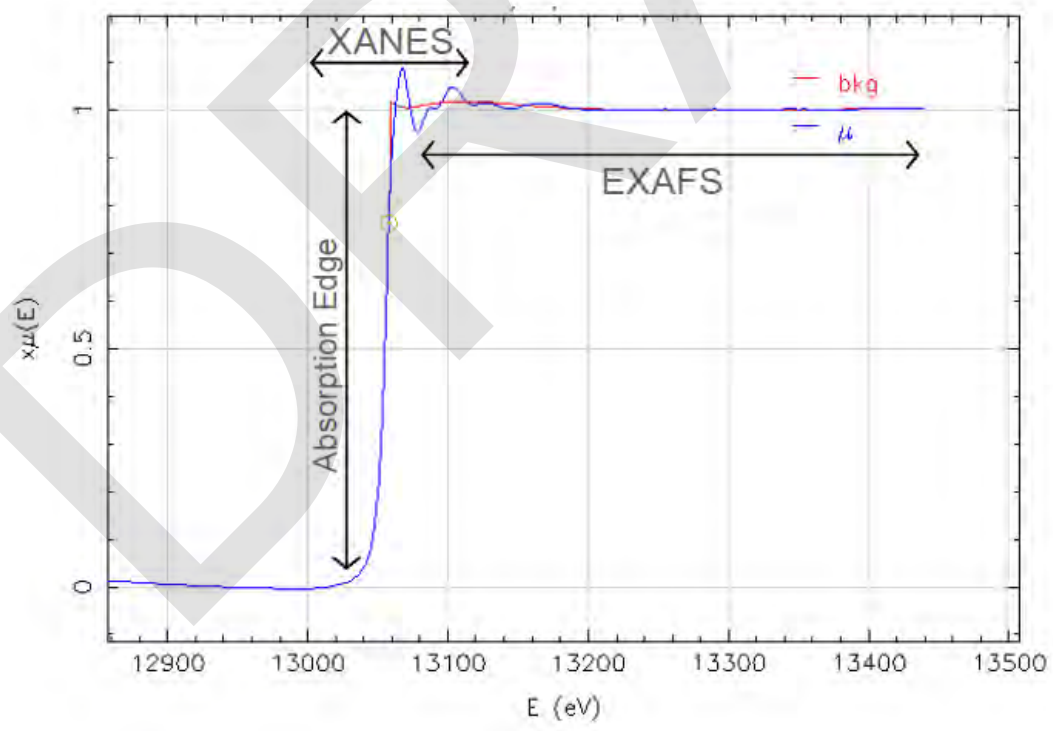

Figure 1. Location of XANES and EXAFS regions of an XAS spectrum. The characteristic energy required to excite core level electrons is unique to each element and is known as the absorption edge or edge step.

The intensity of an X-ray beam as it passes through a material of thickness, t, is given by the absorption coefficient, μ:

$I = I_0 e^{-\mu t}$

where I_0 is the X-ray intensity hitting the material, and I is the intensity transmitted through the material. The absorption coefficient depends strongly on X-ray energy, E, and atomic number, Z, and on the density, μ, and atomic mass, A:

$\mu \approx (Z^4)/(AE^3)$

In addition, μ has sharp absorption edges (Figure 1) corresponding to the characteristic core level energies of the atom. The energies of the K-edge absorption edges go roughly as $E_K \sim Z^2$. All elements with Z>18 have either a K-, or L-edge energies between 3 and 35 keV, which can be accessed at many synchrotron sources.

In many instances for environmental samples, the speciation of metals can result in multiple phases being present. This can make data analysis difficult. For example, EXAFS data analysis is providing information on the average coordination numbers and bond distances for a given element. When multiple species of the same element are present, these parameters are organized into one value that does not represent the complexity of the metal species. The same problem arises when interpreting the coordination environment of metals for XANES data analysis. To overcome this issue, one can apply a statistical fitting procedure that seeks to strip the multiple components of a sample spectrum into individual parts through the assistance of known reference spectra. The two most common methods are linear combination fitting (LCF) and principle component analysis (PCA). LCF

analysis of XANES and XAFS spectra (LCF-XANES and LCF-XAFS) is simple to apply to normalized XANES spectrum or the k^2 or ^{3}-weighted χ-function from EXAFS data reduction. The goal in this procedure is to accumulate enough relevant reference spectra that can explain and represent the unknown environmental sample. Through use of available software, one selects an unknown spectrum to evaluate and multiple known reference spectra to fit against the unknown. By repeating the procedure and removing nonessential reference spectra, one can gain a semi-quantitative analysis of the major metal species present in the unknown sample. Detailed information as collected in EXAFS analysis is not possible but identity of multiple species in the sample is accomplished. For typical environmental samples, LCF-XANES and LCF-XAFS can be a very powerful tool to determine metal speciation when multiple phases are present via a fingerprinting method. This method proves very effective in monitoring contaminated sites to evaluate changes in metal speciation either through in-situ amendments or monitored natural attenuation.

Method

XAS data were collected at the Materials Research Collaborative Access Team (MRCAT) Sector 10, beam line 10-ID, at the Advanced Photon Source (APS) of the Argonne National Laboratory (ANL), U.S. The storage ring operated at 7 GeV in top-up mode. A liquid N_2 cooled double crystal Si(111) monochromator was used to select the incident photon energies and a platinum-coated mirror was used for harmonic rejection. Calibration was performed by assigning the first derivative inflection point of the absorption L_{III}-edge of Pb metal (13035 eV), and each sample scan was collected simultaneously with a Pb metal foil. The samples were ground and pressed into pellets, affixed to a multiport sample holder, and mounted for analysis without any further modifications. Data collection was conducted in fluorescence with an argon filled Lytle detector and in

transmission modes for the samples. For most samples, the transmission data were unusable for analysis. Various Pb standards were used as reference spectra, including inorganic mineral sorbed Pb [Pb-ferrihydrite, Pb-kaolinite, Pb-goethite, Pb-gibbsite, Pb-birnessite, and Pb-montmorillonite in which each mineral was equilibrated with $Pb(NO_3)_2$ at pH 6 for a target surface loading of 2500 mg kg^{-1} after dialysis], organic bound Pb [Pb-fulvic acid and Pb-humic acid as reagent grade organic acids equilibrated with $Pb(NO_3)_2$ at pH 6 for a target loading of 1500 mg kg^{-1} after dialysis, and reagent grade Pb acetate, Pb cysteine, and Pb citrate], Pb carbonate [Smithsonian Natural History Minerals Collection specimens of cerussite, hydrocerussite, and plumbonacrite with X-ray diffraction verification], PbO [massicot and litharge], Pb-phosphates [chloropyromorphite, hydroxypyromorphite, tertiary lead phosphate ($Pb_3(PO_4)_2$), $PbHPO_4$, and Pb sorbed to apatite at pH 6 and surface loading of 2000 mg kg^{-1}], and other lead minerals [leadhillite, magnetoplumbite, plumboferrite, plumbogummite, plumboyarosite, anglesite, and galena from the Smithsonian Natural History Minerals Collection with X-ray diffraction verification]. All reference spectra were collected in transmission mode with dilution calculations determined by XAFSMass (Klementiev, 2012) mixed in binder and pressed into a pellet.

All sample and standard spectra were calibrated to a Pb foil on the same energy grid, averaged, and normalized, and the background was removed by spline fitting using IFEFFIT (Ravel and Newville, 2005). Principal components analyses were performed in Sixpack (Webb, 2005) on the normalized scans, and target factor analyses of each Pb standard were performed to determine the most appropriate standards to be used for linear combination fits (LCF) analyses. Pb standards with SPOIL values <3.0 were used in the LCF analyses, which included mineral sorbed Pb [sum of Pb-ferrihydrite, Pb-goethite, and Pb-birnessite], organic bound Pb [sum of Pb-fulvic acid and Pb-humic acid], Pb carbonate [sum of cerussite and hydrocerussite], and PbO [sum of massicot and litharge.

The k–space functions of the standards and samples were used for all linear combination fitting. Levenberg–Marquardt least squares algorithm was applied to a fit range of 0.6 to 9.0 $Å^{-1}$. Best-fit scenarios, defined as having the smallest residual error, also had sums of all fractions close to 1. To fully describe any particular sample within 1% reproducible error, a minimum of two components was necessary, and results have a ±10% accuracy.

Results and Discussion

The received soils samples were oven dried and sieved to <250 μm prior to XAS analysis. Visual analysis of the samples indicated high levels of organic matter in the sample, typical of forested and grassland areas located at the sites where samples were collected. The results of linear combination fitting of the XAS data are presented below in Table 1.

Table 1. Linear combination fitting results.

	Speciation Distribution (%)		
Sample Label	Organic Matter Bound	Clay/Oxide Sorbed	$\chi 2$ (error)
Pb_K17_001	76	24	0.0206
Pb_K17_002	57	43	0.0114
Pb_K17_003	43	64	0.0242
Pb_K17_004	78	26	0.0116
Pb_K17_005	63	41	0.0090
Pb_K17_006	51	55	0.0201
Pb_K17_007	79	25	0.0057
Pb_K17_008	65	41	0.0151
Pb_K17_009	73	30	0.0086
Pb_K17_010	46	56	0.0097
Pb_K17_011	94	10	0.0166
Pb_K17_012	58	42	0.0567
Pb_K17_013	71	30	0.0365
Pb_K17_014	30	70	0.0218
Pb_K17_015	78	22	0.0347
Pb_K17_016	53	47	0.0553
Pb_K17_017	51	55	0.0294
Pb_K17_018	39	64	0.0269
Pb_K17_019	67	35	0.0710
Pb_K17_001_CDA_OUT	75	25	0.0008
Pb_K17_002_CDA_OUT	66	34	0.0085
Pb_K17_003_CDA_OUT	100	0	0.0292
Pb_K17_004_CDA_OUT	64	36	0.0044

Two primary forms of Pb were identified in the samples where Pb was adsorbed/bounded to organic matter or inorganic clay/metal oxides with the soil samples. Although PCA identified lead oxides as a possible component, its presence in the samples was measured at a maximum of 5% in a handful of samples, and well below the accepted detection limit of 10%. For all the samples, organic matter bound Pb tended to be the most dominant form (~64% on average) relative to Pb adsorption on inorganic soil constituents (~38% on average). Variation of organic matter versus inorganic solid retention of Pb is likely due to surface coverage of degrading plant materials and the presence of silica sand in the soils, which has a very low capacity to adsorb Pb on its surface. Regardless, both primary forms of Pb identified have high potential for release and transport based on previous experience and literature examples.

The impact of Pb attached to the surfaces of organic matter and inorganic clay minerals or metal oxides should be revealed in the in-vitro bioaccessibility (IVBA) results that will likely demonstrate moderate to high IVBA results (50-75%). Follow up speciation analysis after soil amendments are utilized should alter the chemistry of the soil systems and result in different Pb species after reaction.

References

Klementiev, K. V. 2012. XAFSmass, freeware: www.cells.es/Beamlines/CLAESS/software/xafsmass.html

Ravel, B.; Newville, M. ATHENA, ARTEMIS, HEPHAESTUS: data analysis for X-ray absorption spectroscopy using IFEFFIT. *J. Synchrotron Rad*. **2005**, *12*, 537-541.

Smith, E., Kempson, I. M.; Juhasz, A. L.; Weber, J.; Rofe, A.; Gancarz, D.; Naidu, R.; McLaren, R. G.; Grafe, M. In vivo - in vitro and XANES spectroscopy assessments of lead bioavailability in contaminated peri-urban soils. *Environ. Sci. Technol.* **2011**, *45*, 6145-6152.

Webb, S. M. SIXpack: A graphical user interface for XAS analysis using IFEFFIT. *Phys. Scr*. **2005**, *T115*, 1011−1014.

USEPA (1998). Method 3051A, Microwave assisted acid digest of sediments, sludges, soils and oils. In USEPA Methods, pp 3051A/1-24.

RAMBOLL

ATTACHMENT B:
QEMSCAN ANALYSIS OF FOUR SAMPLES FROM THE UPPER COLUMBIA RIVER REMEDIAL INVESTIGATION AND FEASIBILITY STUDY AND BACKGROUND INFORMATION ON QEMSCAN TECHNOLOGY

HAZEN RESEARCH, INC.

HAZEN RESEARCH, INC.

4601 Indiana Street • Golden, Colorado 80403 USA
Phone: (303) 279-4501 • Fax: (303) 278-1528
www.hazenresearch.com

March 30, 2018

Email Delivery

Mr. Dave Enos
SATES Project Coordinator
Teck American Incorporated
501 North Riverpoint Boulevard
Spokane, WA 99202

Subject: QEMSCAN Analysis of Four Samples from the Upper Columbia River Remedial Investigation and Feasibility Study and Background Information on QEMSCAN Technology
Hazen Project 12478
Report and Appendices A–I

Dear Mr. Enos:

This document presents a summary of the mineralogy of four soil samples that were received by Hazen Research, Inc. in October 2017 as part of Teck American Incorporated's Upper Columbia River remedial investigation and feasibility study Soil Amendment Technology Evaluation Study (SATES). The samples reportedly originated from the upper 3 in. of soil profiles. The objective of the analysis was to determine the arsenic and lead mode of occurrences and general soil mineralogy. The investigation focused on the minus 2 mm size fractions of the soil samples.

SUMMARY

Four samples were submitted for analysis:

- D-401-1B-100317-0-3
- D-401-2C-100317-0-3
- D-258-3C-100317-0-3
- D-441-1B-100317-0-3

The samples were scanned automatically using QEMSCAN technology to locate and identify lead- and arsenic-bearing particles. Lead-bearing particles located by the system were fine grained and required manual verification of compositions, sizes, and associations.

Arsenopyrite (FeAsS) was found to be the only arsenic-bearing phase. The most grains were found in Sample D-401-1B. No grains were found in Sample D-441-1B. The observed grain sizes ranged from less than 2 to 250 µm and appeared as angular to subangular slender prisms. All grains observed occurred as free grains. One grain of arsenopyrite was found in Sample D-401-2C, and two grains of arsenopyrite were found in Sample D-258-3C. The maximum size in the latter two samples was 7 µm.

Although arsenopyrite was found to be the only arsenic-bearing phase during the investigation, it is possible that other arsenic-bearing phases may exist. For example, iron oxy-hydroxides, if present, may contain arsenic levels that are too low to be detected by energy-dispersive x-ray spectroscopy (EDS) technology. Organic matter may also contain arsenic at low levels.

Several lead-bearing phases were identified:

- Lead-bearing manganese-rich phase
- Lead–sulfide
- Lead-bearing siliceous glass
- Lead-bearing iron–zinc oxides
- Lead–antimony alloy
- Lead–barium phase

The mode of lead occurrences in each sample is described in this report. The average size of all lead-bearing phases combined was 6 µm (expressed as the equivalent sphere diameter). The phases were too small and irregularly shaped for a comprehensive identification of the nature of the phases and their exact chemical compositions, i.e., the absolute concentration of lead in each phase. Therefore, it was also not possible to determine the distribution of lead between the phases identified. The larger particles containing lead in Sample D-401-1B are manganese-rich. The largest grain size was about 120 by 30 µm.

INTRODUCTION

The four samples (in 10 glass containers) were received on October 6, 2017, in a cooler packed with ice. Upon receipt, the samples were placed in a refrigerator that was kept at a constant 4°C while awaiting work instructions. The samples were also assigned internal tracking numbers (HRI). Work instructions were received from the client on December 1, 2017. Table 1 lists sample names, number of containers per sample submitted, and the as-received sample weights. The weights were determined when sample preparation started (see the Methods section). Sample preparation procedures are outlined in the following section.

Polished sections prepared from subsamples in the minus 2 mm size fraction were analyzed on the Hazen FEI Quanta 650 FEG high-resolution scanning electron microscope (SEM)[1] with QEMSCAN[2] technology.

Table 1. Sample Identifications

Client Sample ID			HRI Number	Number of Containers	Mass Before Drying, g
ID	Date	Time			
D-401-1B-100317-0-3	10/3	12:00	54909-1	3	499.7
D-401-2C-100317-0-3	10/3	11:52	54909-2	2	597.3
D-258-3C-100317-0-3	10/3	14:00	54909-3	3	767.3
D-441-1B-100317-0-3	10/3	15:50	54909-4	2	463.2

METHODS

QEMSCAN TECHNOLOGY

QEMSCAN is an automated mineralogical tool that was selected to determine the general mineralogy of the four soils and to establish how arsenic and lead occur. The system hardware consists of an SEM with a control computer (FEI xT), beam scanning control board, EDS (Bruker X-Flash 6|30), and a data acquisition and processing computer. iDiscover is the name of the entire software suite that is used to operate the QEMSCAN system; gather, manage, and analyze the data; and produce reports. iMeasure is the submodule to control the data acquisition, and iExplorer is the postacquisition processing and analysis module. A report in iExplorer is a plug-in analysis module. It can perform a particular analysis on the sample measurement. Some reports are specialized; others are generalized and can be tailored to perform a wide variety of functions that are specific to the project and the objectives of the investigation.

QEMSCAN uses an electron beam, high-resolution backscatter electron (BSE) imaging and two EDS spectrometers with silicon drift energy-dispersive x-ray detectors (SDD) for analysis. Particles are automatically located within the sample using the contrast in BSE coefficient between the mounting

[1]Electron microscopes use a beam of charged particles and use electromagnetic or electrostatic lenses to focus the beam onto a sample surface. In general, the field emission gun (FEG) electron microscope can see features as small as 10–20 nanometers (1×10^{-8} meter). Electron detectors are used to build an image of the specimen's surface. When electrons impinge on the specimen, they cause, among other phenomena the following: (a) Secondary electrons are emitted by atoms near the surface of a sample. Secondary electron-imaging provides information about sample topography; (b) Some of the primary electrons are reflected backscatter electrons (BSE). The BSE signal is used primarily for its strong atomic number contrast; (c) The impinging electrons may cause specimen atoms to emit x-rays whose energy and wavelength are related to the elemental composition; these are called characteristic x-rays and are used for elemental microanalysis.

[2]QEMSCAN (**Q**uantitative **E**valuation of **M**inerals by **Scan**ning Electron Microscopy) uses advanced electron beam technology and combines this with high-resolution imaging and energy dispersive spectrometry. The components are integrated to provide a comprehensive tool capable of identifying most ore- and rock-forming minerals as well as man-made phases on a microscale in just milliseconds.

medium and the particles. After the particles are located, the electron beam is scanned in a raster-like fashion over the surface at a user-defined stepping interval across the sample (typically 1–25 μm), and x-ray spectra are rapidly acquired. The analyses at each point are correlated with a library of mineral and phase identifications so that each data point is mapped (identified) as a specific mineral or phase. The analysis output is a color-enhanced image with associated quantifiable data.

Two data acquisition modes were used during the current investigation: FieldImage mode and Trace Mineral Search (TMS) routine. Several other modes are available; however, the two modes used are the most appropriate analysis modes.

The FieldImage scan mode captures a full image of each field on the polished section. It is ideal for showing textures and is also used when analyzing samples with unknown sample compositions. Detailed information on mineral associations and grain sizes help in creating or optimizing mineral identification protocols. In the FieldImage mode, the horizontal and vertical analysis point spacing is the same, producing proportional images that can be stitched to produce a composite image montage of areas larger than a single field.

The TMS routine analyzes a preset subpopulation of the particles present. It is based on the premise that the phases of primary interest (i.e., the target phases) have a higher BSE brightness than the bulk of the other minerals that are not of interest. In this instance, lead- and arsenic-bearing minerals were of interest. Because of the higher atomic weights of arsenic and lead, minerals that contain these elements at elevated levels have a relatively high average atomic number and, therefore, appear bright in the BSE image compared with, for example, a silicate-group mineral. The TMS mode enables each polished section to be scanned for particles that contain pixels[3] with BSE brightness levels above a preset level, containing the target phases or other phases with BSE levels above the threshold. Only those particles of interest are fully analyzed. The information obtained from a TMS measurement relates only to the subpopulation of particles analyzed. It provides good statistics on phases of interest in low to trace grade samples because more particles are evaluated in a given time interval.

The QEMSCAN acquisition conditions were as follows:

- 20 kV accelerating voltage
- 10 mA beam current
- 90 kcps[4] pulse throughput to achieve high resolution of spectral peaks and to detect oxygen
- 3.1 μm analysis point spacing in FieldImage mode
- 2 μm spacing in TMS mode
- Field sizes of 757 μm^2 in FieldImage mode and 780 μm^2 in TMS mode

[3]In digital imaging, a pixel is a single picture element in a raster image. In QEMSCAN technology, the pixel size is defined by the stepping interval between EDS analysis points, and is usually measured in μm^2. The spectral information, i.e., chemistry, gathered from the three-dimensional interaction volume of the electron beam with the sample at the point of contact is integrated over the size of the pixel.

[4]kcps = kilocounts per second

- Field sizes of 757 µm^2 in FieldImage mode and 780 µm^2 in TMS mode
- 0.02 s average counting time. Counting time varies and depends on x-ray yields; the total number of x-rays collected, including background counts, was set to 1,000 counts.

The mounting epoxy and pure organic particles have similar average atomic numbers and, therefore, have similar BSE signal levels. They cannot be differentiated from each other and are excluded from the analysis. Mineral matter associated with and incorporated in the cell structures of the organics is detected and analyzed by QEMSCAN. Also, adsorbed elements, like iron, increase the BSE level of the organics above the set BSE threshold value. These areas of organic-rich particles with elevated BSE levels are then also analyzed by QEMSCAN. The mineral abundance results of organics-rich samples can, therefore, be biased because the data may or may not exclude the organic portion.

SAMPLE RECEIPT AND PREANALYSIS PREPARATION

As stated in the Introduction, the four samples were received on October 6, 2017, in two or three glass containers each. The containers were refrigerated at 4°C until further processing.

On December 5, 2017, the sample containers were removed from the refrigerator and photographed. Appendix A shows images of the as-received containers. The individual splits of the samples were weighed, transferred into glass dishes, and then dried overnight at 36°C ± 1°. Table 1 shows the sample weights before drying. The relatively low drying temperature was chosen to avoid dehydrating minerals like gypsum (hydrated calcium sulfate). Appendix B shows the samples inside the drying dishes. After drying, the sample splits were weighed and the weight loss recorded. The splits were then recombined and homogenized.

Sample D-401-1B was processed further as outlined in the following text and analyzed on the QEMSCAN system. The three remaining samples were transferred into plastic jars and stored until the analytical results for Sample D-401-1B were evaluated. This sample was selected by Teck for the initial analysis because it reportedly contained the highest arsenic concentration of the four samples and a relatively high lead level, i.e., 72 ppm As and 2,000 ppm Pb, respectively. Table C1 in Appendix C shows the concentrations of lead and arsenic as reported by Teck.

The following additional sample preparation steps were applied to obtain the fraction for QEMSCAN analysis for each sample:

- The entire sample was screened at 2 mm, and the weight of the plus 2 mm fraction was recorded. At this screening stage, agglomerates of soil and organics were broken apart gently, by hand.
- The plus 2 mm and the minus 2 mm fractions were photographed (see Appendix D).
- The plus 2 mm fraction was archived.
- The minus 2 mm fraction was also photographed (see Appendix D) and stage split using a riffle splitter three or four times (depending on the starting weight of the sample) until a sufficiently small subsplit of the sample mass was obtained.

- The balance of the material from the minus 2 mm fraction was recombined and split in half using the riffle splitter. One split was set aside for possible heavy-liquid separation (HLS), and the second split was archived.
- The minus 2 mm subsplit was then split in eight portions using a Quantachrome rotary splitter. These eight splits were transferred into containers and set aside to prepare polished sections for QEMSCAN analysis and chemical analysis.

While screening Sample D-401-1B at 2 mm, it was observed that the minus 2 mm fraction consisted of fine-grained siliceous soil and an organic fraction that was high in twig content. The estimated grain sizes of the soil were much smaller than 1 mm. The twigs had high aspect ratios, i.e., long axes were considerably larger than 2 mm, and the diameters were smaller than 2 mm. It was hypothesized that the significant organic portion would dilute the inorganic soil portion and would negatively affect the QEMSCAN data acquisition. In consultation with Teck, the minus 2 mm fraction was poured over the 2 mm screen a second time for further separation. The twigs retained on the screen were then collected, weighed, and archived.

The additional rescreening step was not performed in the processing of the three remaining samples because the minus 2 mm fractions of the samples contained higher soil portions and fewer twigs than Sample D-401-1B.

Table E1 in Appendix E lists the as-received and dried sample masses, percentage loss on drying, the mass distributions between plus and minus 2 mm fractions, and the losses during the sample preparation process.

POLISHED SECTION PREPARATION

One subsplit of the bulk minus 2 mm fraction of each sample was mounted as round epoxy blocks (28 mm in diameter). When the epoxy set, the mounts were ground on grinding discs with decreasing grit sizes and polished using diamond suspensions, also with decreasing particle sizes down to a 1 µm size. The sections were carbon coated to render the surfaces conductive under the negatively charged electron beam of the SEM.

For Sample D-401-1B, a polished section of the HLS sink fraction was also prepared for the QEMSCAN study (see the Heavy-Liquid Separation section).

QEMSCAN DATA ACQUISITION

Initial QEMSCAN Data Acquisition

The polished section of the bulk minus 2 mm fraction of Sample D-401-1B was scanned in the FieldImage and the TMS modes. After reviewing the results, Teck refined the scope of work to include an evaluation of the high-density particle fraction of the sample (see the Heavy-Liquid Separation section).

Heavy-Liquid Separation and Final Data Acquisition

Teck instructed Hazen to perform an HLS on one of the half splits of the minus 2 mm fraction of Sample D-401-1B because it was hypothesized that lead- and arsenic-bearing phases would be concentrated in the sink fraction. The results were negative. Based on the results, only the polished sections of the bulk minus 2 mm fractions of the three remaining samples were analyzed.

HEAVY-LIQUID SEPARATION

An HLS was performed on a split of about 140 g of the minus 2 mm fraction of Sample D-401-1B without desliming. Separation was performed using acetylene tetrabromide, with a specific gravity of 2.92 in a separation funnel. The sink and float fractions were filtered, washed with acetone, and dried. The sink fraction was split in half. One split was used to prepare a polished section, and the second split was archived. The mass distribution between sink and float fractions is in Table F1 in Appendix F.

CHEMICAL ANALYSES METHODOLOGY

Huffman Hazen Laboratories performed chemical analyses on the organic-rich portion and final minus 2 mm fraction of Sample D-401-1B. As outlined in the Sample Receipt and Preanalysis Preparation section, the organic-rich portion of the minus 2 mm fraction was obtained by rescreening the initially obtained minus 2 mm fraction at 2 mm to retain as many twigs as possible on the screen. The organic-rich portion of the minus 2 mm fraction represented 4% of the total sample mass (after drying), and the final minus 2 mm fraction represented 71% of the total sample after drying. Both fractions were analyzed for total sulfur on a LECO S-1444DR combustion instrument. Lead was analyzed by inductively coupled plasma–optical emission spectrometry; arsenic, antimony, tin, bismuth, barium, selenium, and zinc were analyzed by inductively coupled plasma–mass spectrometry. The analytical report is in Appendix G.

RESULTS

This section describes the results of the study and includes the following topics:

- Observations made during the sample preparation process
- Chemical analyses of the minus 2 mm fraction of Sample D-401-1B after removal of an organic-rich portion and the organics
- Mineralogy of the bulk minus 2 mm fractions of the four samples and the characterization of the HLS sink fraction
- Arsenic and lead assemblages

SAMPLE CHARACTERISTICS

Table E1 in Appendix E lists the as-received and dried sample masses, percentage loss on drying, the mass distributions between plus and minus 2 mm fractions, and the losses during the sample preparation process.

The mass loss on drying at 36°C ranged from 5.2 to 8.6%. The highest moisture content was observed in the sample with the highest portion in the minus 2 mm fraction (D-258-3C). In general, the samples exhibited a wide range of particle sizes, from pebble (several centimeters in size) to ultrafine dust. The top particle sizes of Samples D-401-2C and D-441-1B were larger than the other two samples (see images in Appendix D). The portion of the plus 2 mm fraction ranged from 4 to 48%. A distinct organic component, consisting of roots, leaves, twigs, and bark, was present in all samples. Charcoal particles were also observed in all samples. The prevalent sample color was dark brown. During the handling of the samples (sieving and splitting), ultrafine, blackish dust formation was widespread. The dust covered working surfaces, containers, tools, and splitters. It was difficult to minimize formation and contain the dust. Some of the losses during handling were attributed to the dust formation.

CHEMICAL ANALYSES

Chemical analyses were performed on only two fractions of Sample D-401-1B, i.e., an organic-rich subfraction of the minus 2 mm fraction (4.3 mass% of the total sample on a dry sample basis) and the final minus 2 mm fraction after removal of the organic portion (71.2 mass% on a dry basis). The analytical report is in Appendix G. The concentrations of total sulfur, lead, antimony, tin, bismuth, selenium, and zinc are higher in the organic-rich fraction than the minus 2 mm fraction, whereas the levels of arsenic and barium are lower. The lead concentrations of the organic-rich fraction and the minus 2 mm fraction were 0.152 and 0.115%, respectively. The arsenic concentrations in these fractions were 21 and 55 ppm, respectively. These levels of lead and arsenic were lower than the concentrations of the bulk sample reported by Teck, i.e., 2,060 ppm Pb and 71.6 ppm As (see Appendix C).

MINERALOGICAL CHARACTERIZATION OF MINUS 2 mm FRACTIONS BY QEMSCAN

Mineral Abundance Analysis on Bulk Minus 2 mm Fraction

Table 2 shows the mineral abundance results of the four sample size fractions analyzed. Figure 1 shows the data as a bar graph. The results were normalized and excluded the organic portion present in the minus 2 mm fractions. As outlined previously, pure organic matter is almost entirely excluded from QEMSCAN analyses because of the low BSE signal intensity.

Low levels of the identified lead- and arsenic-bearing phases were included in the mineral abundance analysis. The mode of occurrence of lead and arsenic are detailed in the Lead and Arsenic Assemblages section.

Quartz and feldspar (plagioclase and K-feldspar) totaled between 73 and 85 mass% of the minus 2 mm fractions. Muscovite ($KAl_2AlSi_3O_{10}(OH,F)_2$) and biotite ($K(Mg,Fe)_3AlSi_3O_{10}(OH,F)_2$) micas, clinochlore

($(Mg,Fe)_5Si_3Al_2O_{10}(OH)_8$, a mineral of the chlorite group), and possibly talc ($Mg_3Si_4O_{10}(OH)_2$) were observed. Their combined concentrations varied between 4.2 and 9.2%. The group labeled "other silicates" in Table 2 contained amphibole- or pyroxene-group minerals, or both, garnets, and kaolinite clay. Other minerals observed were apatite (calcium phosphate), titanium oxide, iron oxide and hydroxides, carbonate (mainly ankerite ($Ca(Fe,Mg,Mn)(CO_3)_2$), monazite (rare earth phosphate), barite (barium sulfate), and iron sulfide). Other unspecified silicates, other sulfides, and glass were grouped under the "miscellaneous" category in Table 2. All measurement points that could not be classified as one of the phases mentioned above were grouped as "unidentified." The group may contain small concentrations of yet-unidentified phase or phases, but most likely consists of the already identified phases, at the respective measured proportions of all identified phases in a given sample or fraction.

Figure 2 is an example montage of individual fields (306) of the QEMSCAN acquired data with color-enhanced mineral identification. Each color represents a different mineral or group of minerals. The map illustrates particle sizes and shapes and mineral intergrowth textures. The maps of the minus 2 mm fractions of the four samples are in Appendix H.

Mineral Abundance Analysis on Heavy-Liquid Separation Sink Fraction

Because of the low concentration of lead-bearing phases in the bulk minus 2 mm size fraction of Sample D-401-1B, Teck requested Hazen to perform an HLS on a split of the minus 2 mm fraction and analyze the sink fraction on the QEMSCAN system. The separation was performed at 2.92 sg using acetylene tetrabromide. The sink fraction represented 4.1% of the minus 2 mm size fraction (see Table F1 in Appendix F).

Table 3 shows the mineral abundance results of the sink fraction. The data are compared with the concentrations of the minerals present in the bulk 2 mm size fraction of the sample. Figure 3 shows the QEMSCAN particle map. The list of minerals identified is more detailed than the mineral list used in Figure 2 of the bulk fraction, where low-level phases were grouped.

Only isolated pixels of lead- and arsenic-bearing phases were detected during the automated data acquisition. The compositions of these pixels were verified manually. None of the pixels were found to be lead or arsenic bearing.

The sink fraction was relatively coarse grained (75–600 µm) and consisted mainly of iron–oxides, monazite, apatite, garnet, amphibole-group minerals, and zircon.

The absence of lead-bearing phases in the sink fraction suggested that the sample probably did not contain any coarse-sized lead-bearing phases and that the lead-bearing phases present reported to the fines or the float fraction, or both. Separation is less effective when grains are very small. As part of the HLS procedure, the sink and float fractions were washed with acetone. Fractions were collected on filter paper. Fines may be lost within the filter paper fibers.

Table 2. Mineral Abundance of Minus 2 mm Fractions

Client sample ID	D-401-1B	D-401-2C	D-258-3C	D-441-1B
HRI number	**54909-1-5**	**54909-2-5**	**54909-3-5**	**54909-4-5**
Mineral	**Mass, %**			
Pb-bearing	0.08	0.02	0.004	0.02
Arsenopyrite	0.08	0.0003	0.001	0.0003
Fe sulfides	0.03	0.001	0.001	0.001
Quartz	32	33	35	19
Feldspar	49	46	50	54
Mica–chlorite–talc	5.1	8.5	4.2	9.2
Other silicates	9.2	9.0	8.5	11.0
Apatite	0.3	0.3	0.2	1.2
Barite	0.003	0.0005	0.0002	0.0004
Rutile or anatase	0.1	0.2	0.2	0.1
Fe–(Ti) oxides	2.2	2.0	0.9	1.6
Ce-phosphate (monazite)	0.02	0.01	0.01	0.02
Carbonate	0.1	0.04	0.05	0.1
Organics[a]	0.1	0.03	0.02	0.1
Miscellaneous	0.4	0.5	0.2	0.9
Unidentified	1.4	1.1	0.7	2.6
Total	**100**	**100**	**100**	**100**

Note: the results are normalized and exclude the main portion of the organics reporting to the minus 2 mm fraction.
[a]The reported mass of organics in the table represents only a portion of the total organics reporting to the size fraction. The organics were analyzed because of elevated BSE signal levels.

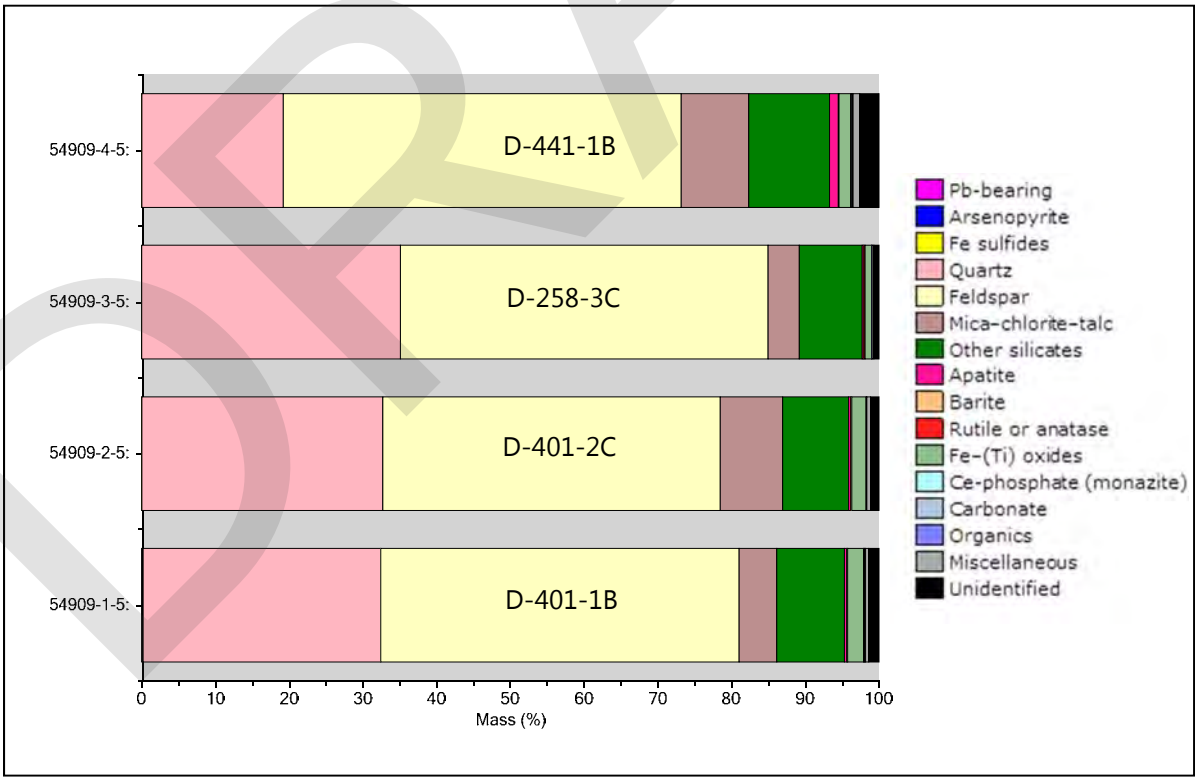

Figure 1. Bar Graph of Mineral Abundance Data of Minus 2 mm Fractions

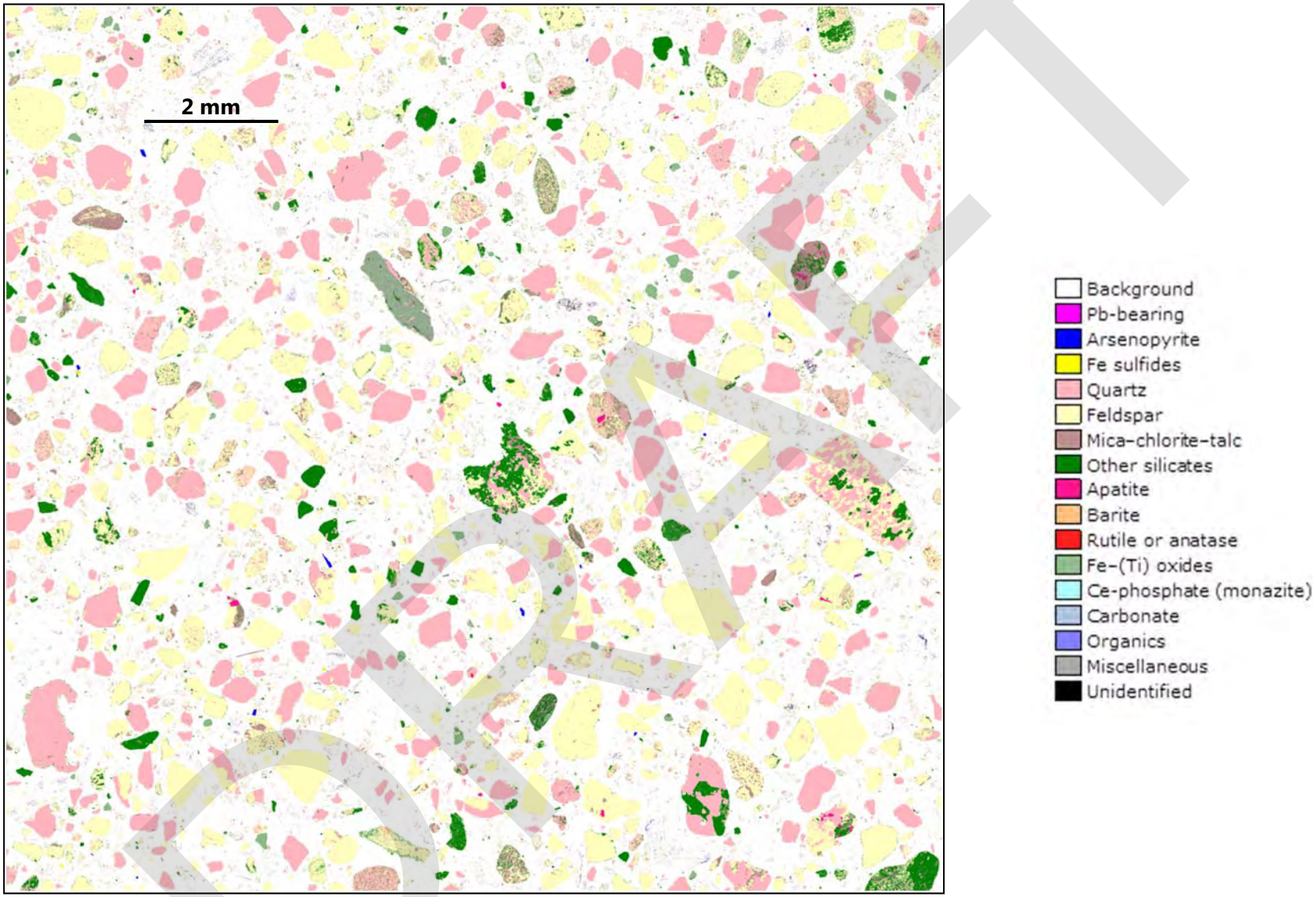

Figure 2. QEMSCAN Color-Enhanced Particle Map Montage of Center Area Analyzed on Polished Section of D-401-1B (minus 2 mm fraction)

Table 3. Comparison of Mineral Abundance Analysis of Bulk Minus 2 mm Fraction and Heavy-Liquid Separation Sink Fraction

Client sample ID	D-401-1B less than 2 mm	D-401-1B less than 2 mm Sink
HRI number	**54909-1-5**	**54909-1-5-Sink**
Mineral	**Mass, %**	
Pb-bearing	0.08	0.01
Arsenopyrite	0.08	0.0003
Fe sulfides	0.03	0.02
Fe–Zn–O	0.01	0.06
Quartz	32	1.1
Feldspar	49	2.6
(Na)–Ca–Al silicate	0.2	0.04
Muscovite	2.7	0.4
Biotite	0.6	0.3
Chlorite-group mineral	1.8	0.5
Talc	0.0	0.1
Amphibole and pyroxene	4.1	8.8
Garnets	1.8	18.4
Staurolite	0.1	0.6
Andalusite or kyanite or sillimanite	0.1	1.4
Epidote	1.1	1.4
REE-bearing silicate	0.1	1.1
Apatite	0.3	0.7
Rutile or anatase	0.1	1.0
Fe–(Ti) oxides	2.2	42.0
Titanite	0.3	2.3
Tourmaline	0.06	0.05
Kaolinite (clay)	1.1	0.4
Zircon	0.04	2.6
Ce-phosphate (monazite)	0.02	11.7
Miscellaneous	0.7	1.8
Unidentified	1.4	0.8
Total	**100**	**100**

REE = rare earth element

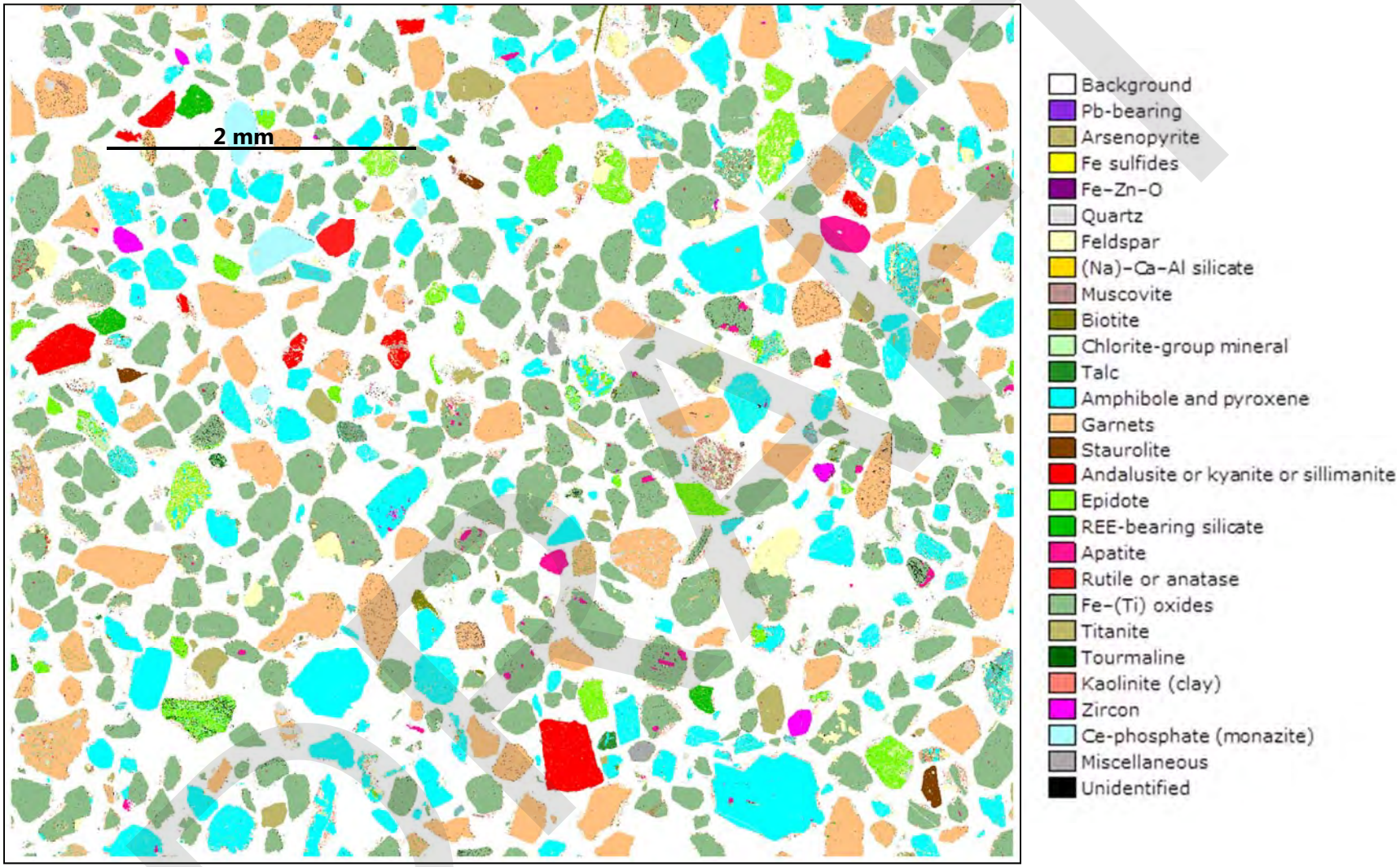

Figure 3. QEMSCAN Color-Enhanced Particle Map of Center Area Analyzed on Polished Section of the Heavy-Liquid Separation-Sink Fraction of D-401-1B (minus 2 mm fraction)

Lead and Arsenic Assemblages

The polished sections of the four minus 2 mm fractions were analyzed by QEMSCAN in the TMS mode to automatically locate lead- and arsenic-bearing phases. As Table 2 shows, the measured levels were low. Sample D-401-1B exhibited the highest concentrations, i.e., 0.08% each for lead- and arsenic-bearing phases. The concentrations in the other three samples were considerably lower. During the data evaluation, it was also observed that a portion of the apparent lead- and arsenic-containing pixels were misidentified by the software. Incorrect identification during fast data acquisition is possible when grains are smaller than the excitation volume[5] of the method, when intergrowth textures are very fine, or when the analysis point falls on the edge of a particle or on a hole or a surface scratch.

Actual lead-bearing phases were found to be fine grained, which increased the uncertainty of automated mineral identification. Therefore, all arsenic- and lead-bearing pixels were verified manually. The following sections describe the mode of occurrences observed.

Arsenic Assemblages

Sample D-401-1B

Arsenopyrite (FeAsS) was found to be the only arsenic-bearing phase in this sample. Figure 4 shows the arsenopyrite particles identified by QEMSCAN. Arsenopyrite appeared as angular to subangular slender prisms. The observed grain sizes ranged from less than 2 to 250 µm (as longest axis). All arsenopyrite grains observed occurred as free grains. The grains were sorted by area percent of arsenopyrite. The observed associations with other minerals in Figure 4 are a coincidental physical closeness of two independent particles.

In QEMSCAN technology, the size of a mineral is an estimate of the diameter of the particles in a population. The value is the diameter of a sphere of equivalent volume to the average grain in the

[5]Interaction of the electron beam with atoms in the sample causes inner electron shell transitions, which result in the emission of x-rays. Two types of x-rays are generated: (1) bremsstrahlung or continuous x-rays, which generate a background over the entire spectrum, and (2) element-specific x-rays, which form discrete peaks in the spectrum and whose energies are characteristic of specific elements present at the point of analysis.

X-rays derive from deeper in the sample than both secondary and BSE. The volume of the specimen in which x-rays are produced and detected is relatively large because x-rays penetrate matter far more readily than electrons. The interaction volume depends strongly on the energy of the primary electron beam, the density of the specimen (which is, to a certain degree, controlled by the average atomic number (Z) of the specimen) and the specific element that is analyzed. High electron beam energies and low-Z targets result in large interaction volumes. The effective depths (three-dimensional) from which sulfur and lead x-rays can originate when analyzing, for example, a lead sulfide grain, which has an average specific gravity of 7.4, and applying a 20 keV beam, are approximately 2.6 and 1.7 µm, respectively. For particles with sizes smaller than the theoretical excitation volume, the x-ray signals are barely above the background noise level or are obscured by the x-ray signals generated by the surrounding phases or the mounting resin. It can be concluded that the error associated with the identification and quantification of fine grains increases with decreasing grain size.

population. For the arsenopyrite population in Sample D-401-1B, the size expressed as the equivalent sphere diameter (ESD) measured 40 µm.

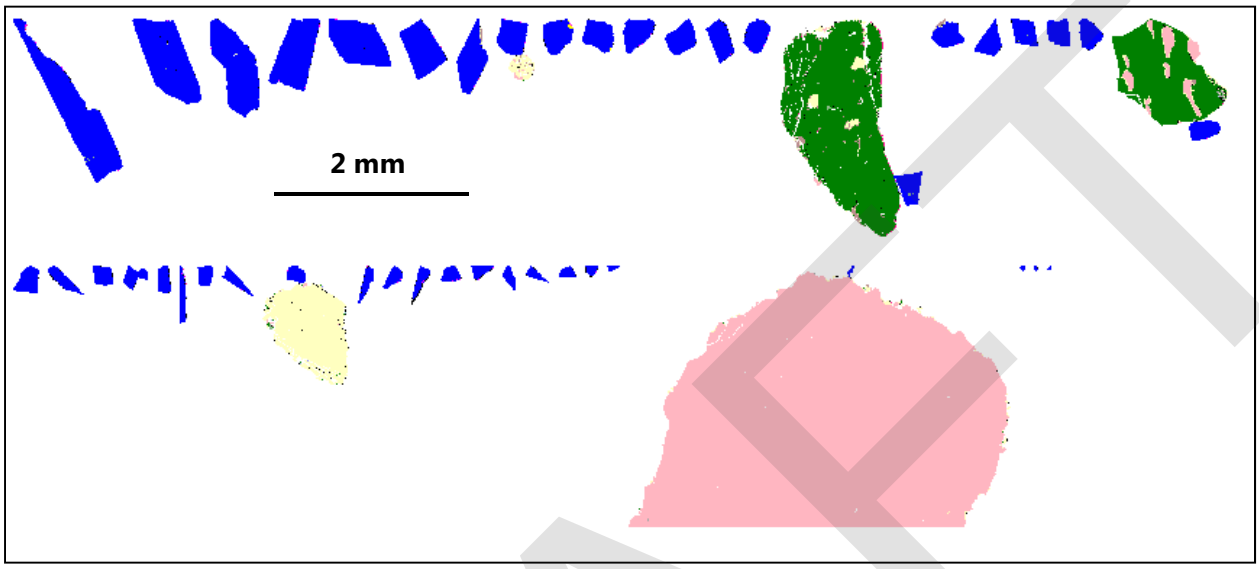

Note: The blue is arsenopyrite, light yellow is feldspar, pink is quartz, and green is other silicates.

Figure 4. Arsenopyrite Grains Observed in Sample D-401-1B Detected by QEMSCAN

Sample D-401-2C

Only a single grain of free arsenopyrite (4 µm) was observed in the sample. A BSE image of the grain is in Figure 5.

Sample D-258-3C

Only two grains of arsenopyrite were observed during the TMS run (5 and 7 µm). The BSE images of the grains are in Figures 6 and 7.

Sample D-441-1B

No arsenic-bearing grains were observed during the manual verification of the QEMSCAN TMS data.

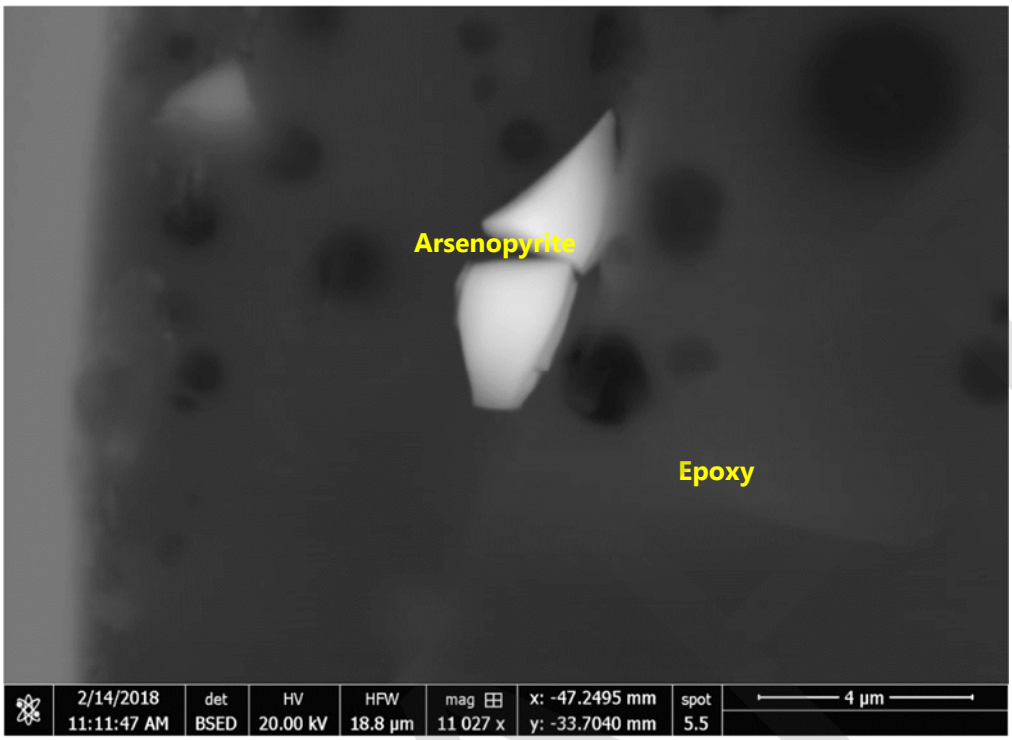

Figure 5. Backscatter Electron (atomic number contrast) Image of Arsenopyrite Grain in Sample D-401-2C

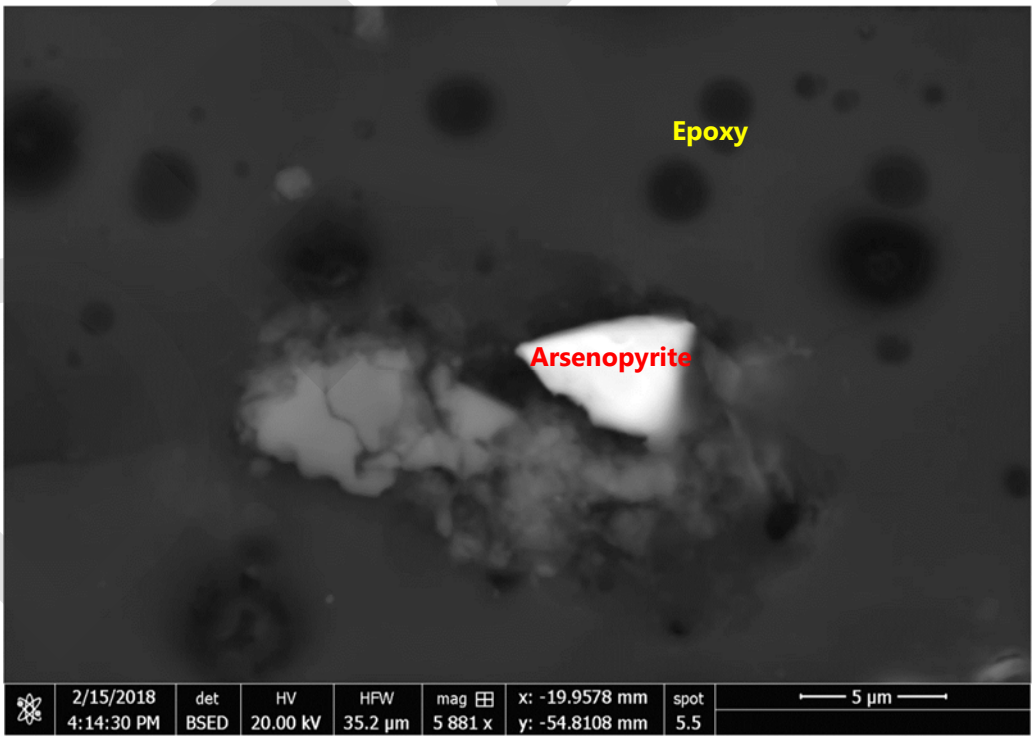

Figure 6. Backscatter Electron Image of Arsenopyrite Grain 1 in Sample D-258-3C

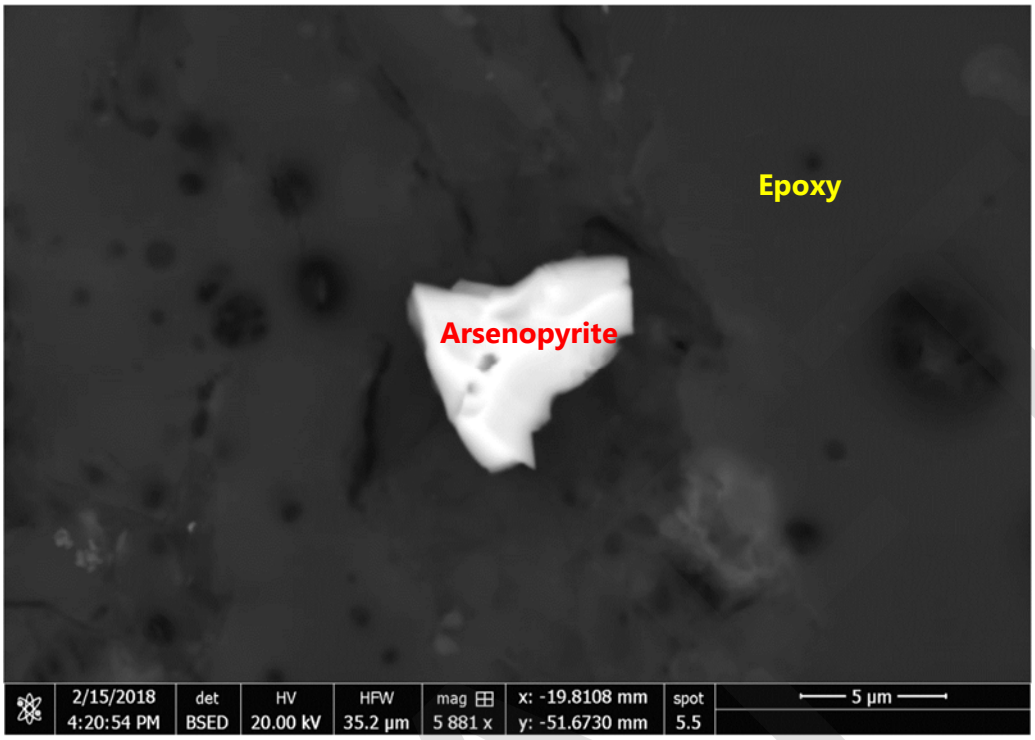

Figure 7. Backscatter Electron Image of Arsenopyrite Grain 2 in Sample D-258-3C

Lead Assemblages

During the initial study on the mode of occurrences of lead in Sample D-401-1B, several lead-bearing phases were identified. These phases are listed in Table 4, in no particular order. The phases were characterized by the elements detected in the EDS x-ray spectra.

Table 4. Lead-Bearing Phases Identified in Sample D-401-1B

Pb-Bearing Phases
Galena (PbS)
Pb–Si glass
Pb–Sb-bearing
Pb–Ba-bearing
Pb–Ba–S-bearing
Fe–Pb–O
Fe–Pb–S–O
Mn–Pb–O
Pb–Al–Si–O glass
Fe–Zn–Pb–O
Other Pb-bearing
Pb–Sb–Sn

The average ESD size of all lead-bearing phases combined was less than 6 µm. The phases were too small and irregularly shaped to comprehensively identify the nature of the phases and their exact chemical compositions, i.e., the absolute concentration of lead in each of the phases. Therefore, it was also not possible to determine the distribution of lead between the phases identified. The following sections describe the main observations related to the lead-bearing phases in each sample.

Sample D-401-1B

The larger particles containing lead in Sample D-401-1B are irregularly shaped particles that are rich in manganese and that also contain zinc, iron, titanium, oxygen, and other elements. The largest manganese–lead-bearing grain was about 120 by 30 µm. Figure 8 shows an example of one of the manganese-rich particles. Other examples are in Appendix I (Figures I1–I3).

Sample D-441-2C

Lead was observed as part of various phases:

- As a lead–silicon–oxygen phase (up to 20 µm), possibly glass
- As a lead-bearing aluminum–silicon–oxygen phase, possibly glass
- As a lead-bearing iron–zinc–oxygen phase with variable levels of lead
- As a lead–antimony alloy
- At low levels of lead in iron oxide
- As barium–lead sulfate associated with organics
- At low levels of lead in iron–manganese–titanium-rich layer on feldspar

The average size of lead-bearing phases (expressed as ESD) was about 4 µm. It was not possible to quantify the lead concentrations in each of the phases because the particles were too small. Examples of BSE images of the lead-bearing phases are in Appendix I (Figures I4–I16).

Sample D-258-3C

Lead was observed as part of three phases:

- As a lead-bearing manganese-rich phase, predominantly associated with organics or possibly charcoal (possibly adsorbed onto the surface of organics)
- At low levels in an iron–zinc–oxygen phase
- As an unidentified lead-rich phase associated with siliceous material (possibly glass)

The average size (expressed as ESD) was about 5 µm. The largest lead-bearing grain was about 25 by 15 µm. It was not possible to quantify the lead concentrations in each phase because the particles were too small. Examples of BSE images of the lead-bearing phases are in Appendix I (Figures I17–I28).

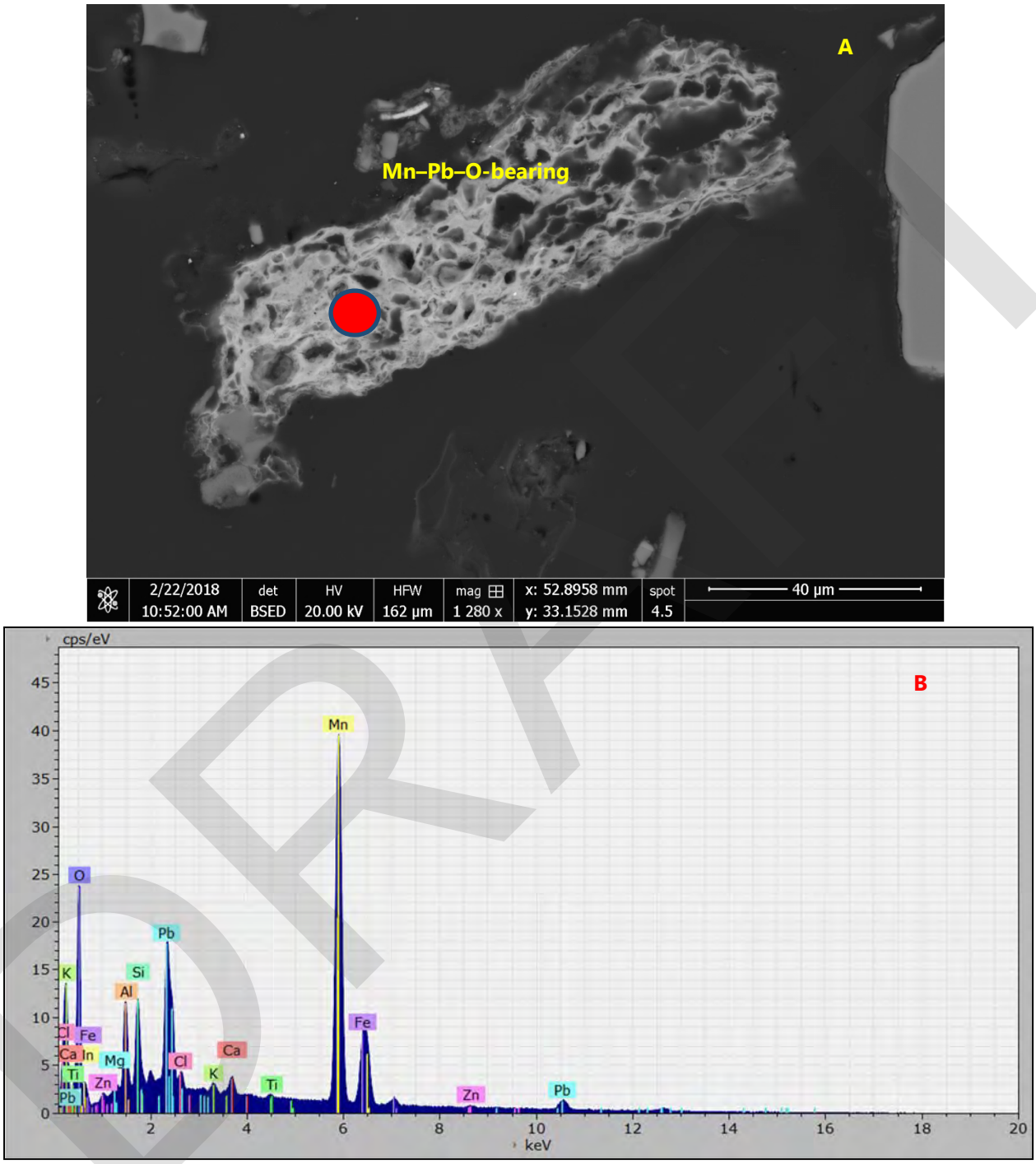

Figure 8. Backscatter Electron Image (A) and Screenshot of Energy-Dispersive X-Ray Spectrum (B) Acquired in Vicinity of Red Spot in A – Sample D-401-1B

Sample D-441-1B

Lead was observed as part of four different phases:

- As a lead-bearing manganese-rich phase, predominantly associated with organics or possibly charcoal (possibly adsorbed onto the surface of organics)
- At low levels of lead in iron–zinc–oxygen
- As a single occurrence of a spherical particle consisting of lead–zinc–cadmium–silicon phase
- As a lead–antimony alloy

The average size (expressed as ESD) was about 5 µm. It was not possible to quantify the lead concentrations in each of the phases because the particles are too small. Examples of BSE images of the lead-bearing phases are in Appendix I (Figures I29–I41).

LIMITATIONS AND CAVEATS OF ANALYSIS

QEMSCAN technology is ideal to scan entire polished sections in a relatively short time and locate target particles of specific chemical compositions down to about 1–3 µm, thus providing information on millions of data points. If expected particles of interest are smaller than 1 µm, the overall acquisition time to cover the surface of an entire polished section increases because of tighter analysis point stepping intervals or the area that can be scanned in a given time frame is limited. A selective area analysis may not be representative of the entire exposed particle population in a polished section.

Analyzing only one polished section of samples or size fractions with a broad-particle size range (in this instance, 2 mm to less than 1 µm) can lead to a bias in particle data. The representativeness of data decreases with increasing average particle size.

Analyzing broad-range size fractions can also lead to possible particle or mineral segregation during the preparation of polished sections. This segregation is influenced by particle sizes and densities.

Knowledge of expected particle size ranges and compositions of the phases of interest would assist in determining suitable sample preparation procedures and data acquisition parameters. If this information is not available, the initial investigation can become something like a needle-in-the-haystack search. Chemical analyses of size fractions obtained from screening the broad minus 2 mm fraction into six to eight subfractions, including a minus 38 µm fraction, would be beneficial.

As outlined in the report, the quality of EDS analyses of fine-grained target particles that are smaller than the excitation volume from which x-rays are collected can be low, which in turn increases the uncertainty of identification. The information on the modes of occurrence of lead and arsenic presented in this report is qualitative because the data population is too small.

Hazen hopes these results are beneficial to you. If you have any questions, please contact me at your convenience.

Regards,

Hanna Horsch
Manager, Quantitative Mineralogy

HH/gr

xc: Denise Mills, Teck American Incorporated (email: denise.mills@teck.com)
Cristy Kessel, Teck American Incorporated (email: cristykessel@teck.com)
Mike Arnold, Ramboll Group A/S (email: marnold@ramboll.com)
Amy Kephart, Ramboll Group A/S (email: akephart@ramboll.com)
Roland Schmidt, Hazen Research, Inc.
Nick Hazen, Hazen Research, Inc.

APPENDIX A

Sample Container Images

Figure A1. Sample D-401-1B in Glass Containers As-Received

Figure A2. Sample D-401-2C As-Received

Figure A3. Sample D-258-3C As-Received

Figure A4. Sample D-441-1B As-Received

APPENDIX B

Images of Samples in Drying Containers

Figure B1. Sample D-401-1B in Drying Dish

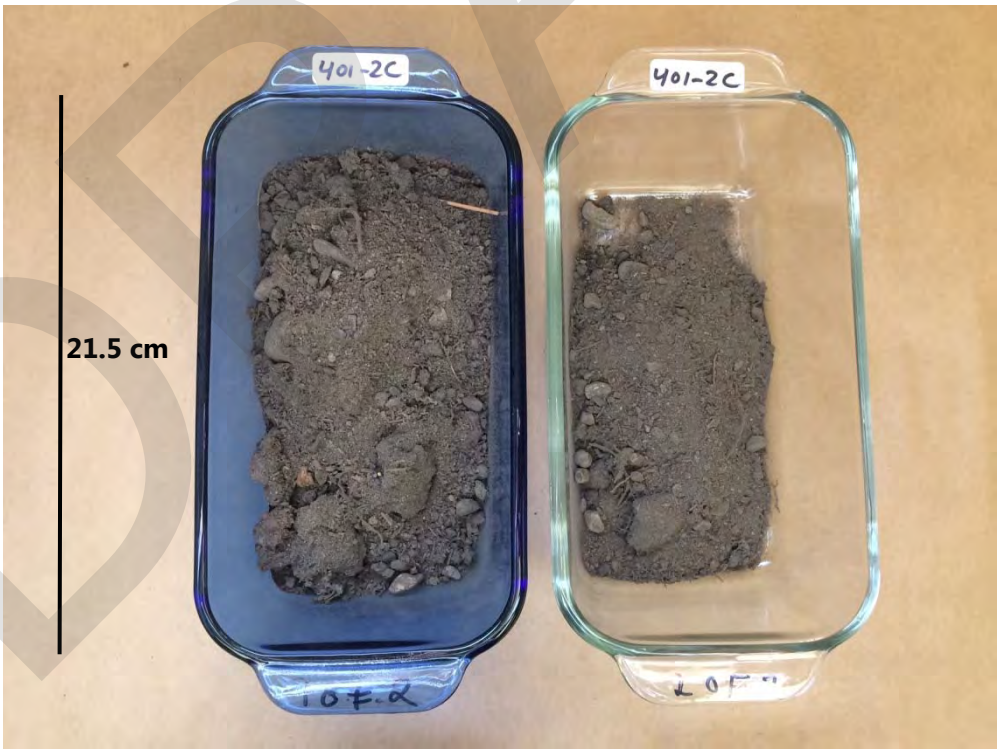

Figure B2. Sample D-401-2C in Drying Dish

Figure B3. Sample D-258-3C in Drying Dish

Figure B4. Sample D-441-1B in Drying Dish

APPENDIX C

Expected Concentrations (table provided by Teck)

Table C1. Estimated Concentrations of Bulk Samples as Reported by Teck

Sample ID	Lead mg/kg DryWt	Arsenic mg/kg DryWt
D-401-1B-100317-0-3	2060	71.6
D-401-2C-100317-0-3	1800	65.3
D-258-3C-100317-0-3	2350	14.8
D-441-1B-100317-0-3	2150	30

APPENDIX D

Images of Screen Fractions

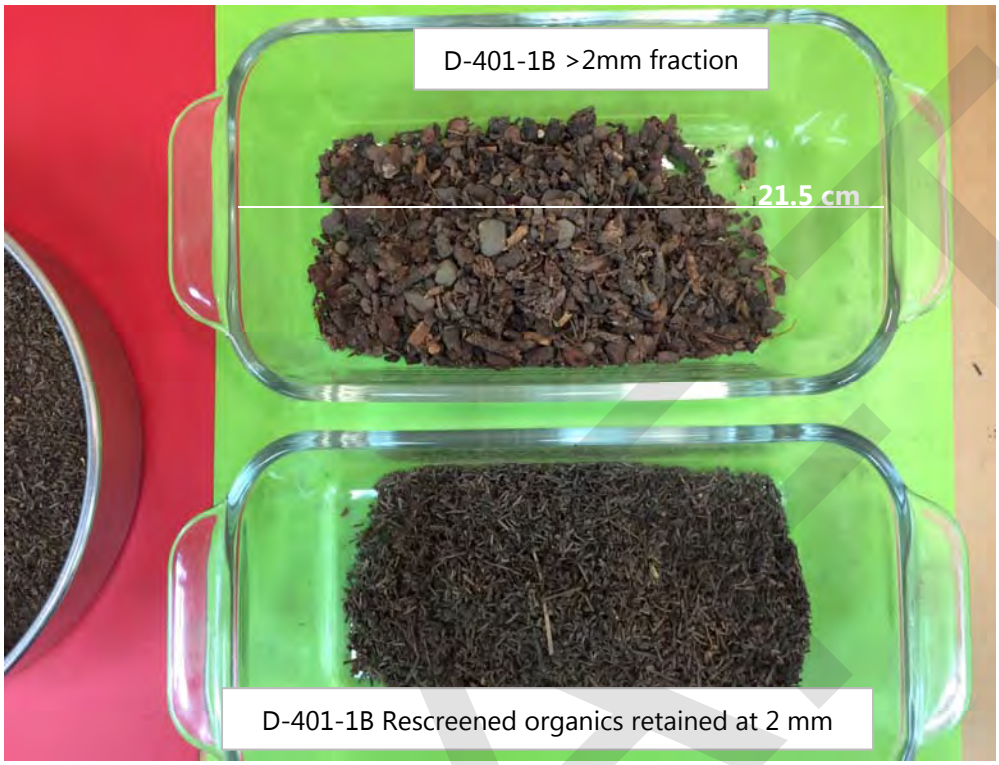

Figure D1. Plus 2 mm Fraction and Rescreened Organic Fraction of Sample D-401-1B

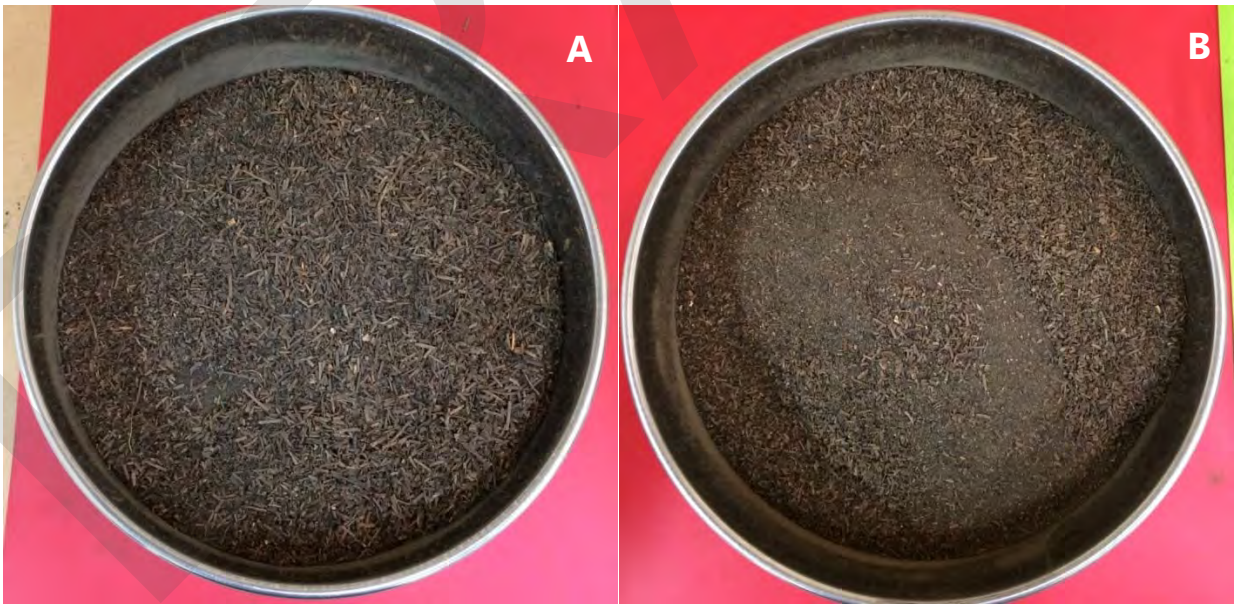

Figure D2. Minus 2 mm Fraction Before (A) and After (B) Rescreening, D-401-1B

Figure D3. Plus 2 mm fraction of Sample D-401-2C

Figure D4. Minus 2 mm Fraction of D-401-2C

Figure D5. Plus (left) and Minus (right) 2 mm Fractions of D-258-3C

Figure D6. Plus (left) and Minus (right) 2 mm Fractions of D-441-1B

APPENDIX E

Sample and Fraction Weights

Table E1. Sample Weights

Client Sample ID	D-401-1B-100317-0-3	D-401-2C-100317-0-3	D-258-3C-100317-0-3	D-441-1B-100317-0-3
Hazen Sample ID	**54909-1**	**54909-2**	**54909-3**	**54909-4**
Mass before drying, g	499.7	597.3	767.3	463.2
Mass after drying,[a] g	467.4	570.7	701.2	438.9
Loss on drying, %	6.5	4.5	8.6	5.2
Mass of >2 mm fraction, g	114.4	212.9	29.3	207.7
Organics,[b] rescreened at 2 mm, g	19.9	none	none	none
Total >2 mm, g	134.3	212.9	29.3	207.7
Mass of <2 mm fraction, g	331.7	354.2	666	228.4
Total sample, g	466	567.1	695.3	436.1
Loss during sample preparation, g	1.4	3.6	5.9	2.8
>2 mm, %	29	38	4	48
<2 mm, %	71	62	96	52

[a]Dried at 36°C ±1

[b]Minus 2 mm fraction was rescreened at 2 mm to remove organic material with a large aspect ratio

APPENDIX F

Heavy-Liquid Separation Analysis

Table F1. Heavy Liquid Separation at 2.92 sg using Acetylene Tetrabromide

Client Sample ID	**D-401-1B-100317-0-3 <2mm**
Hazen Sample ID	**54909-1-5**
Starting mass, g	138.7
Mass in float fraction, g	131.2
Mass in sink fraction, g	5.6
Total	**136.8**
Loss during HLS, g	-1.9
Float fraction, %	95.9
Sink fraction, %	4.1
Total minus 2 mm, %	**100**

APPENDIX G

Analytical Report

Hazen Research, Inc.
4601 Indiana Street
Golden, CO 80403 USA
Tel: (303) 279-4501
Fax: (303) 278-1528

Lab Control ID: 18H01008
Received: Jan 05, 2018
Reported: Jan 23, 2018
Charge Code: 433

Customer ID: 38029H
Account ID: Z00573
Project #: 12478

Hanna Horsch
Hazen Research, Inc.
4630 Indiana Street
Golden, CO 80403

ANALYTICAL REPORT

Analytical services provided by:
Huffman Hazen Laboratories
A Division of Hazen Research, Inc.
4630 Indiana Street, Golden, CO 80403
phone: 303-278-4455

This report is intended only for the named customer and/or recipient approved by the customer. If you have received this report in error please return it to Huffman Hazen Laboratories

By: Sandy Kanapilly
Lab Manager

Hazen Research, Inc.
4601 Indiana Street
Golden, CO 80403 USA
Tel: (303) 279-4501
Fax: (303) 278-1528

Lab Control ID: 18H01008
Received: Jan 05, 2018
Reported: Jan 23, 2018
Charge Code: 433

Customer ID: 38029H
Account ID: Z00573
Project #: 12478

Hanna Horsch
Hazen Research, Inc.

ANALYTICAL REPORT

Lab Sample ID	Customer Sample ID	Sulfur % w/w	Lead µg/g	Arsenic µg/g	Antimony µg/g	Tin µg/g
18H01008-001	54909-1-4	0.16	1520	21	66	8.5
18H01008-002	54909-1-5	0.08	1150	55	55	7.5

Lab Sample ID	Customer Sample ID	Bismuth µg/g	Barium µg/g	Selenium µg/g	Zinc µg/g
18H01008-001	54909-1-4	3.1	248	1.7	900
18H01008-002	54909-1-5	2.3	660	1.0	714

The samples were ground prior to analysis.

Sample ID

54909-1-4: D-401-1B-100317-0-3 12:00: Organic-rich portion of minus 2 mm fraction. The fraction was obtained by rescreening the original minus 2mm at 2 mm. The organic-rich portion represents 4% of the total sample (after drying at 36°C).

54909-1-5: D-401-1b_100317-0-3 12:00: Minus 2 mm fraction after removal of the organic-rich portion (54909-1-4). Fraction 54909-1-5 represents 71% of the total sample after drying.

APPENDIX H

QEMSCAN Particle Maps

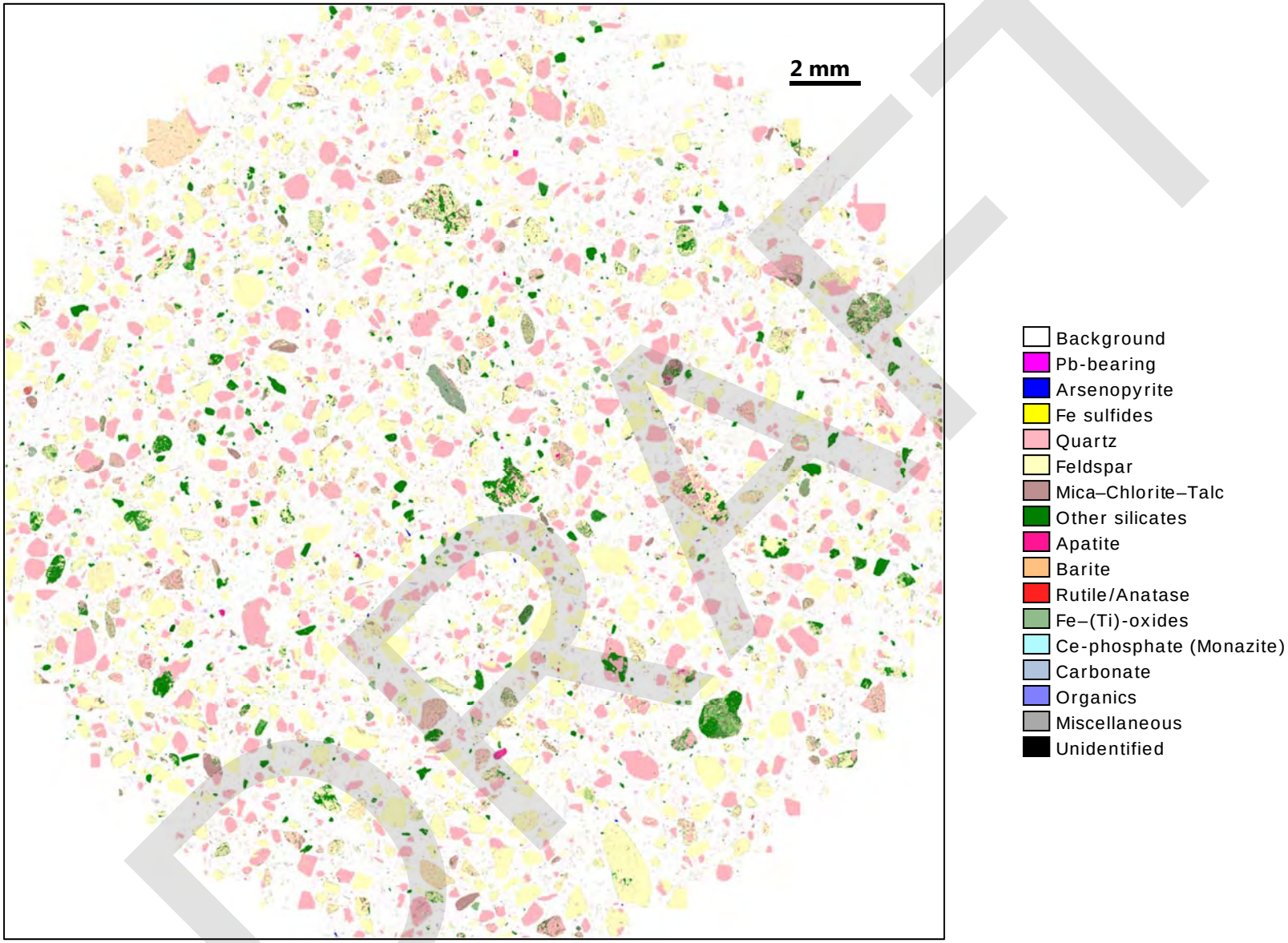

Figure H1. Color-Enhanced Particle Map of Minus 2 mm Fraction of D-401-1B

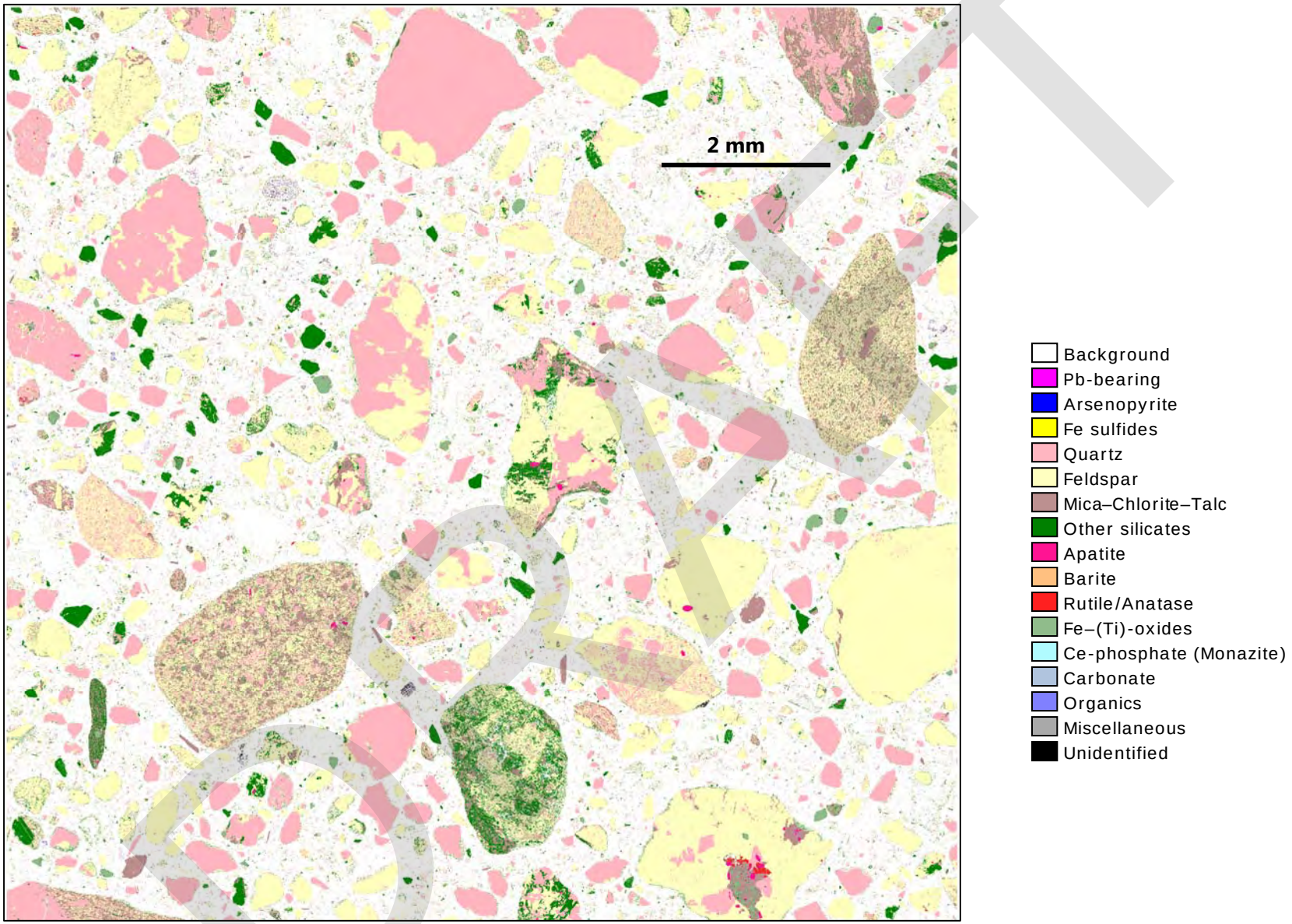

Figure H2. Color-Enhanced Particle Map of Minus 2 mm Fraction of D-401-2C

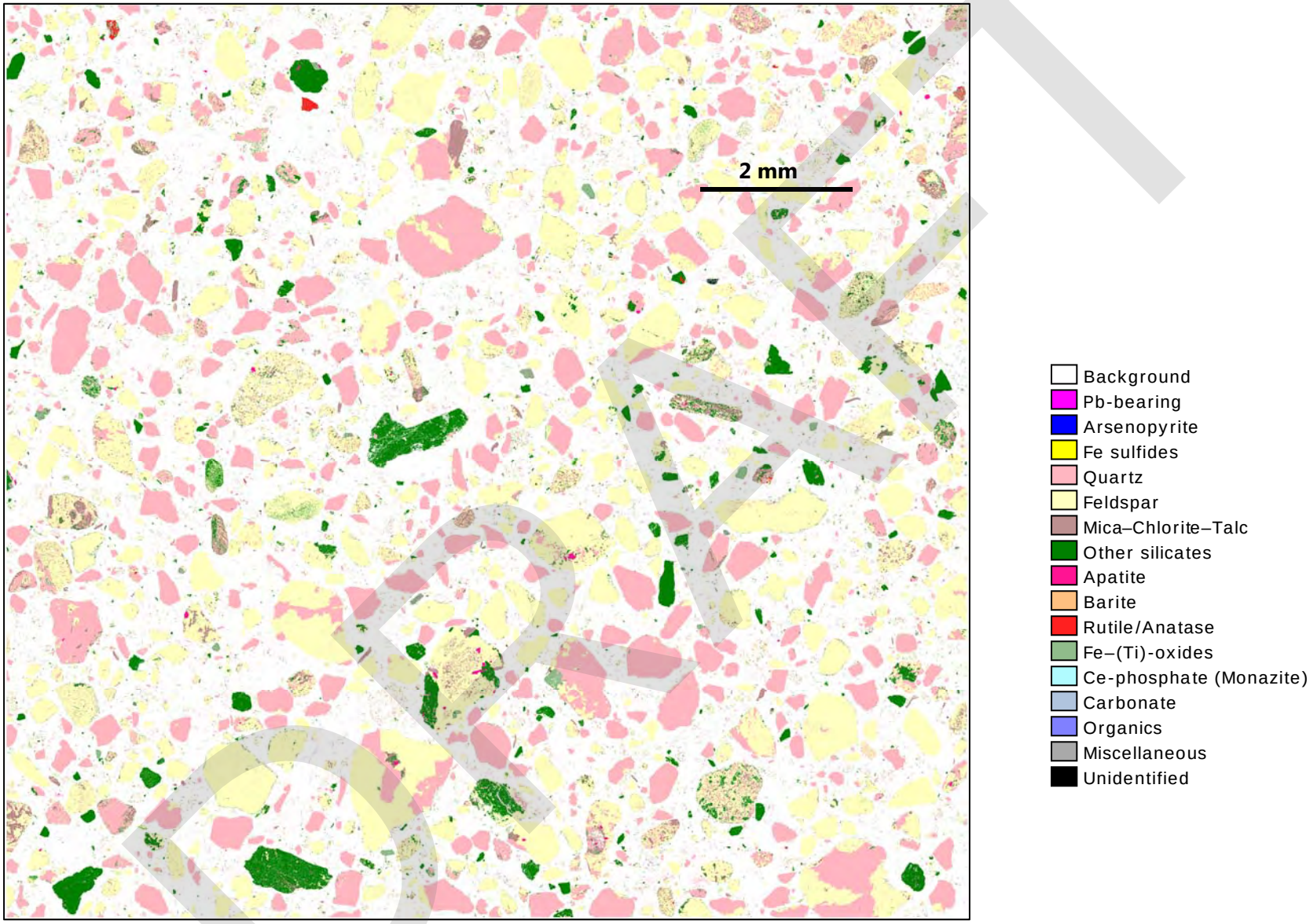

Figure H3. Color-Enhanced Particle Map of Minus 2 mm Fraction of D-258-3C

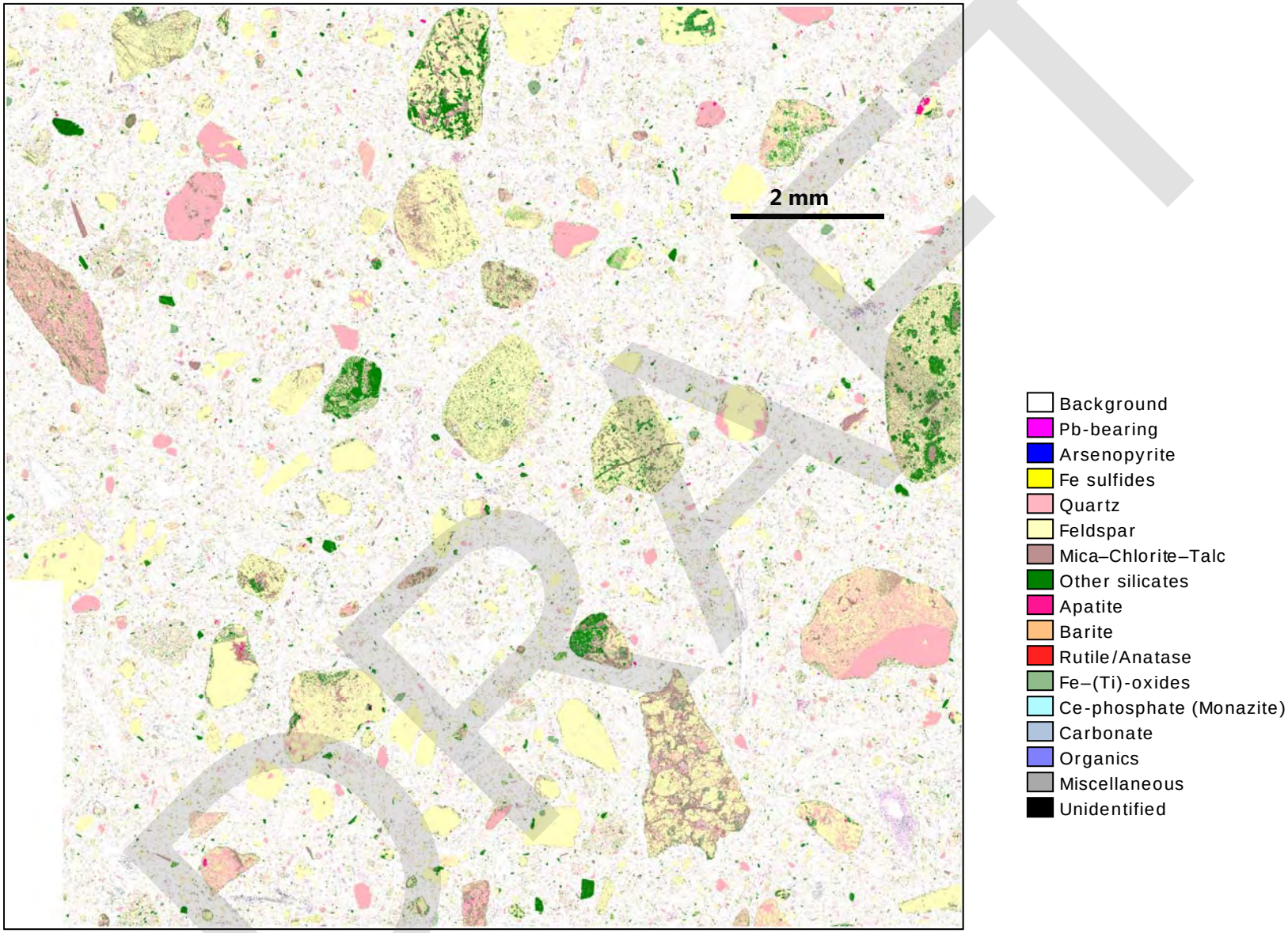

Figure H4. Color-Enhanced Particle Map of Minus 2 mm Fraction of D-441-1B

APPENDIX I

Examples of Backscatter Electron Images of Lead-Bearing Particles

Note: All images were acquired on particles observed in the polished sections of the minus 2 mm size fractions.

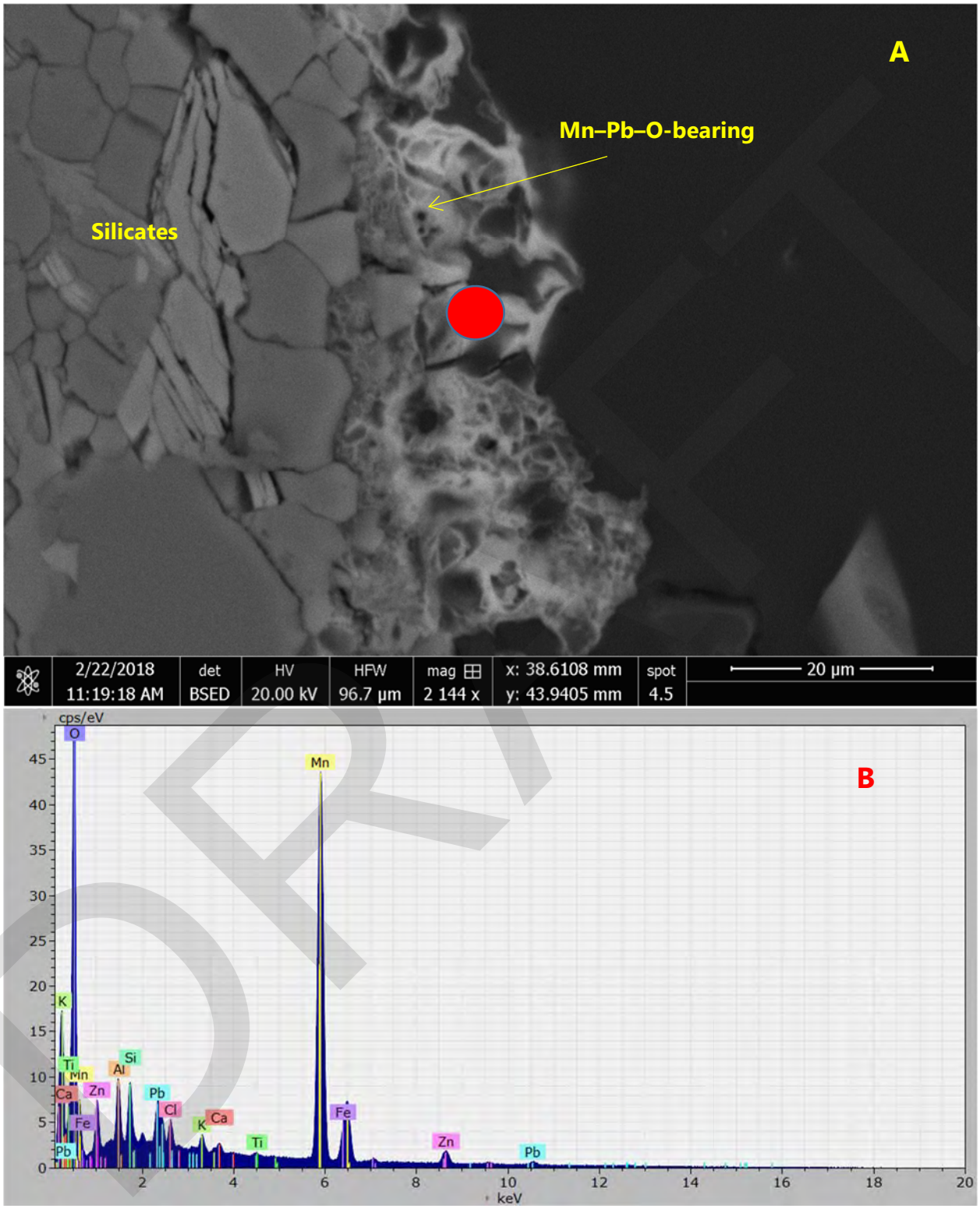

Figure I1. BSE Image (A) of Pb-Bearing Mn-Rich Phase and Screenshot of EDS X-Ray Spectrum (B) Acquired on Red Spot Marked in (A) – Sample D-401-1B, Example 1

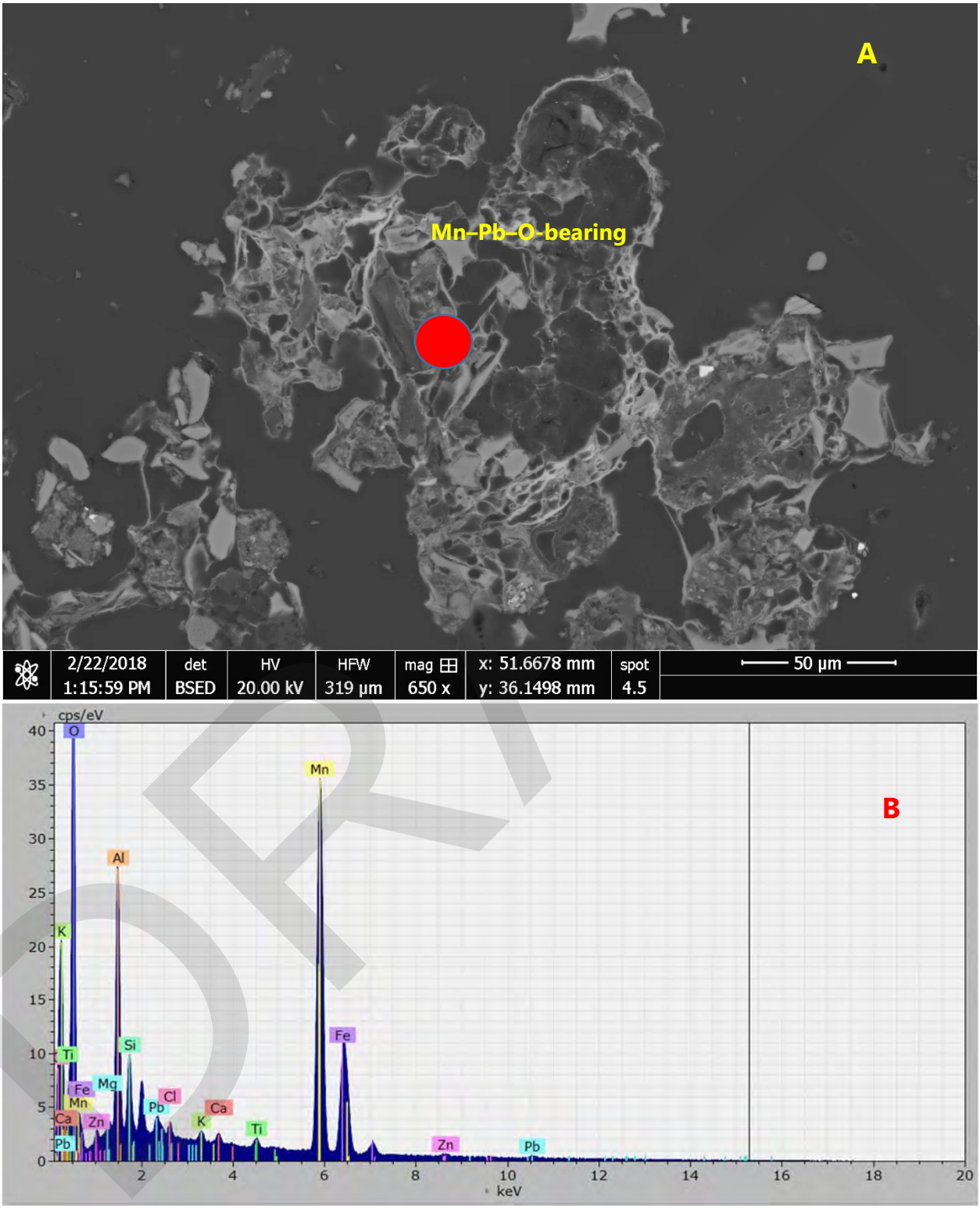

Figure I2. BSE Image (A) of Pb-Bearing Mn-Rich Phase and Screenshot of EDS X-Ray Spectrum (B) Acquired on Red Spot Marked in (A) – Sample D-401-1B, Example 2

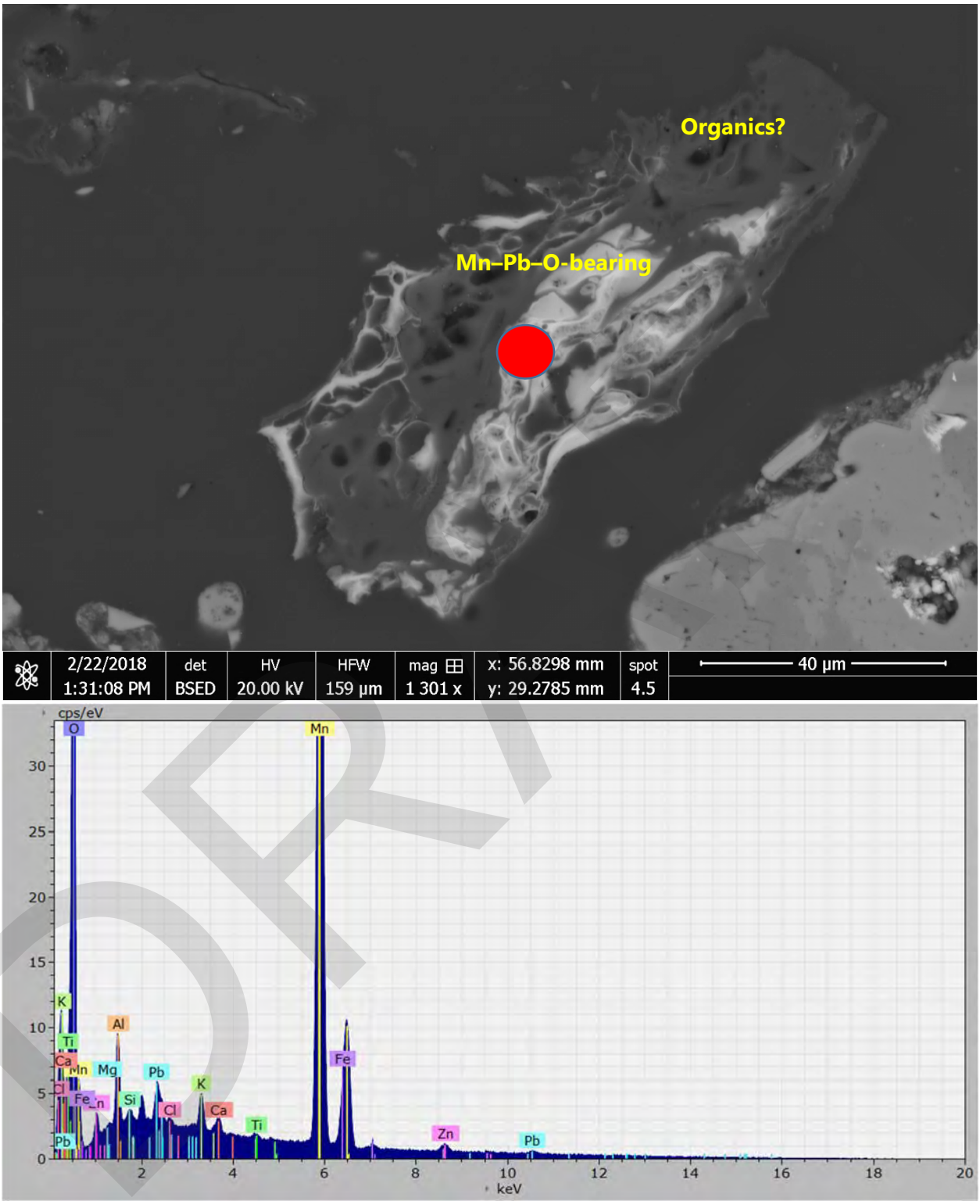

Figure I3. BSE Image (A) of Pb-Bearing Mn-Rich Phase and Screenshot of EDS X-Ray Spectrum (B) Acquired on Red Spot Marked in (A) – Sample D-401-1B, Example 3

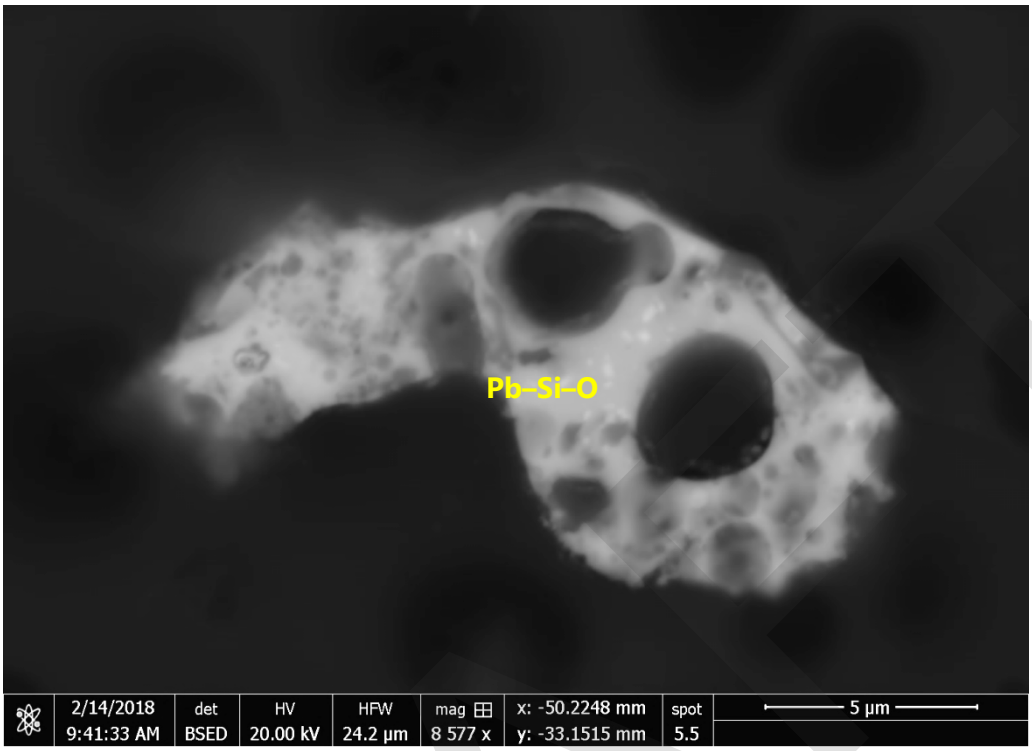

Figure I4. BSE Image of Pb-Bearing Glass in Sample D-401-2C, Example 1

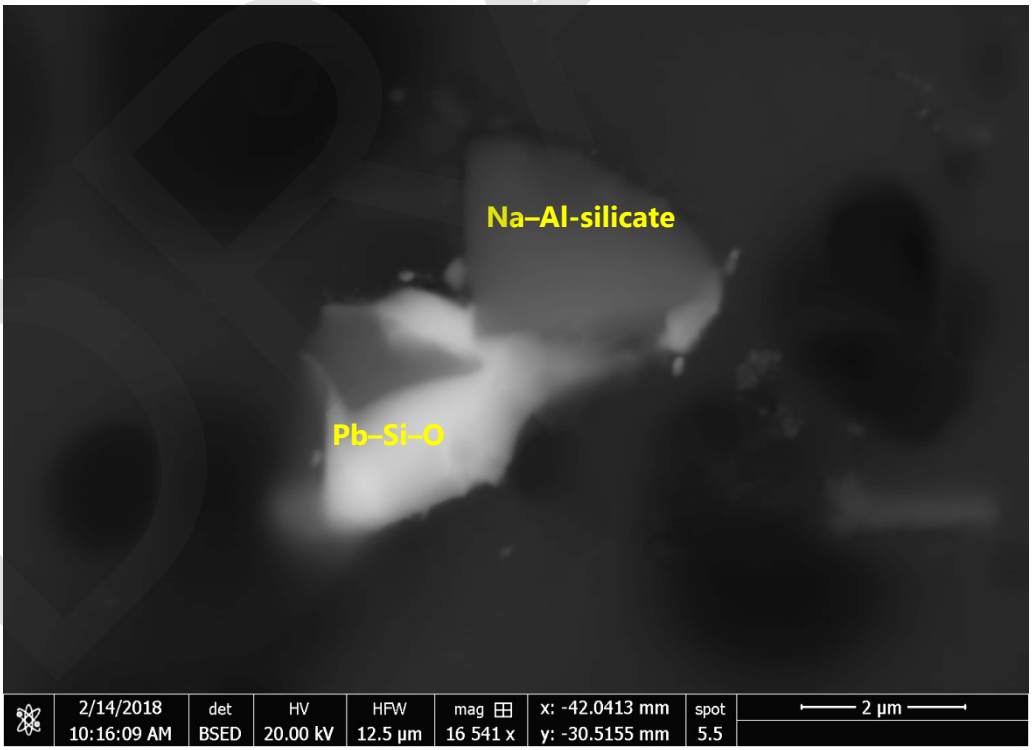

Figure I5. BSE Image of Pb-Bearing Glass in Sample D-401-2C, Example 2

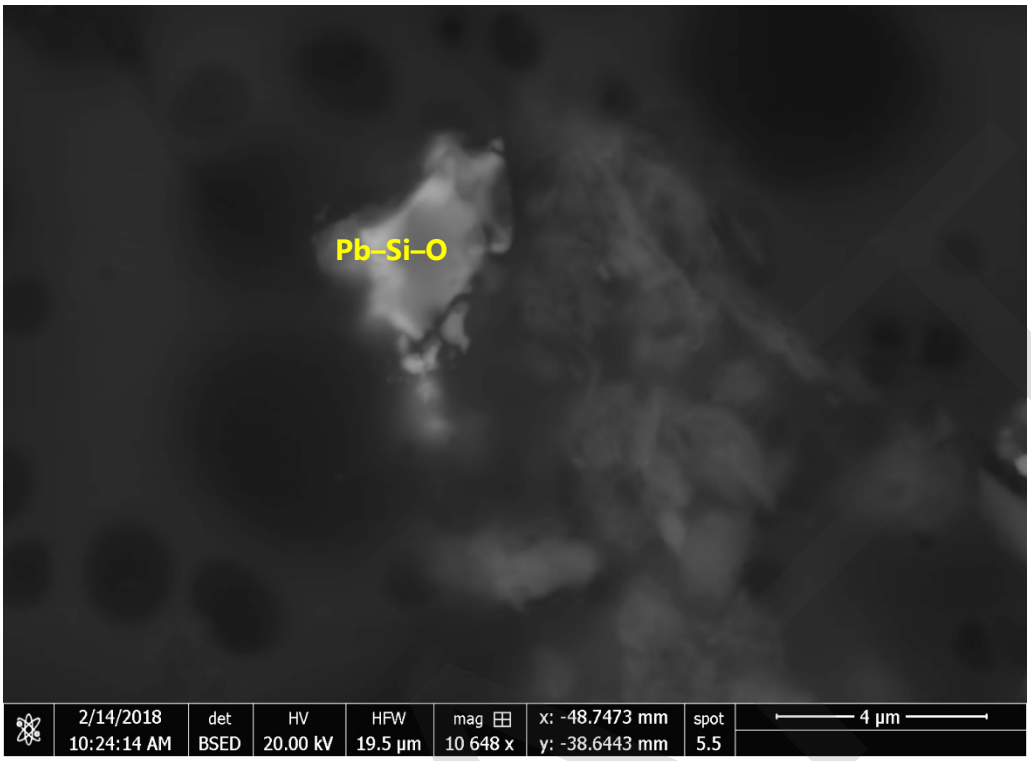

Figure I6. BSE Image of Pb-Bearing Glass in Sample D-401-2C, Example 3

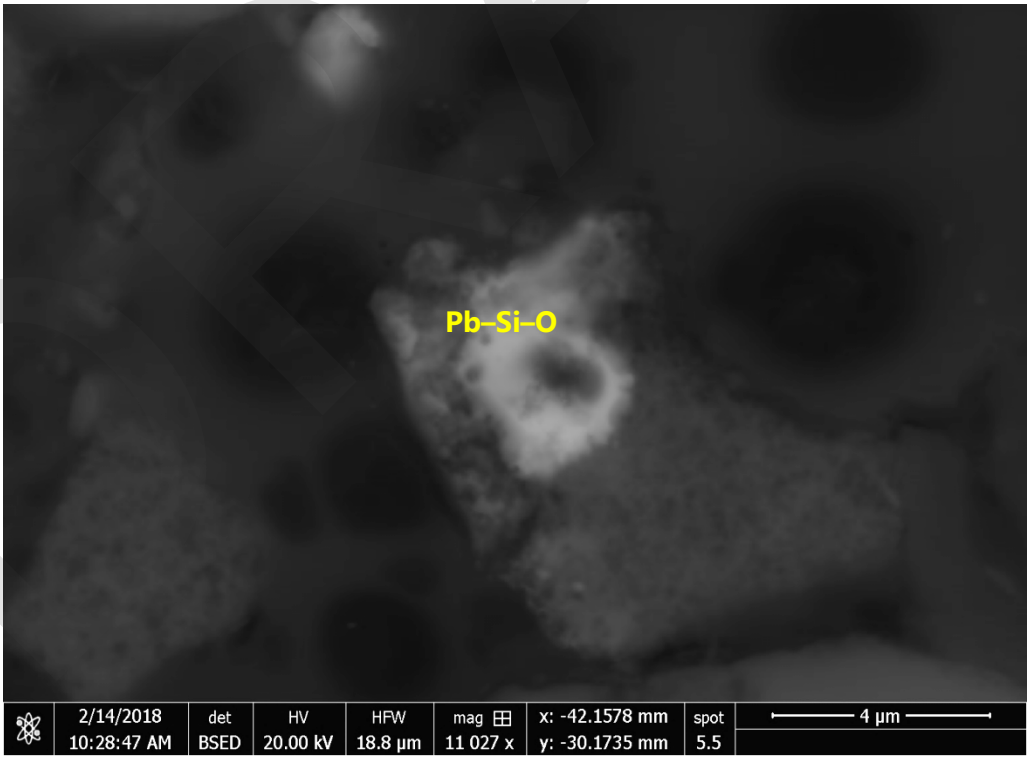

Figure I7. BSE Image of Pb-Bearing Glass in Sample D-401-2C, Example 4

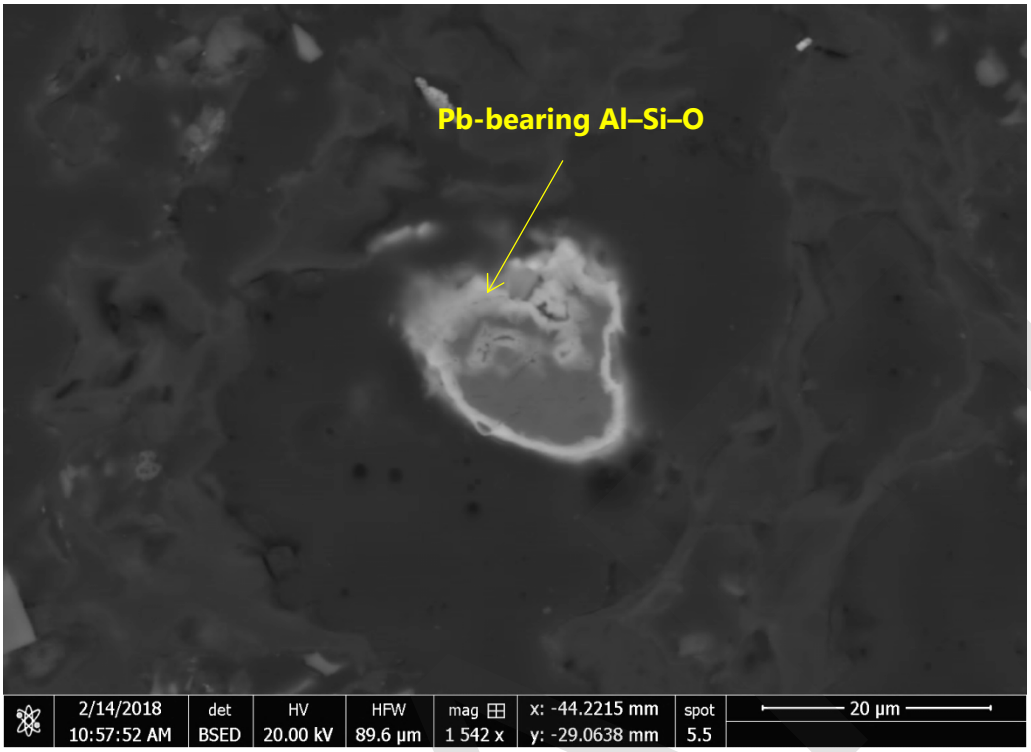

Figure I8. BSE Image of Pb-Bearing Al–Si–O Glass in Sample D-401-2C

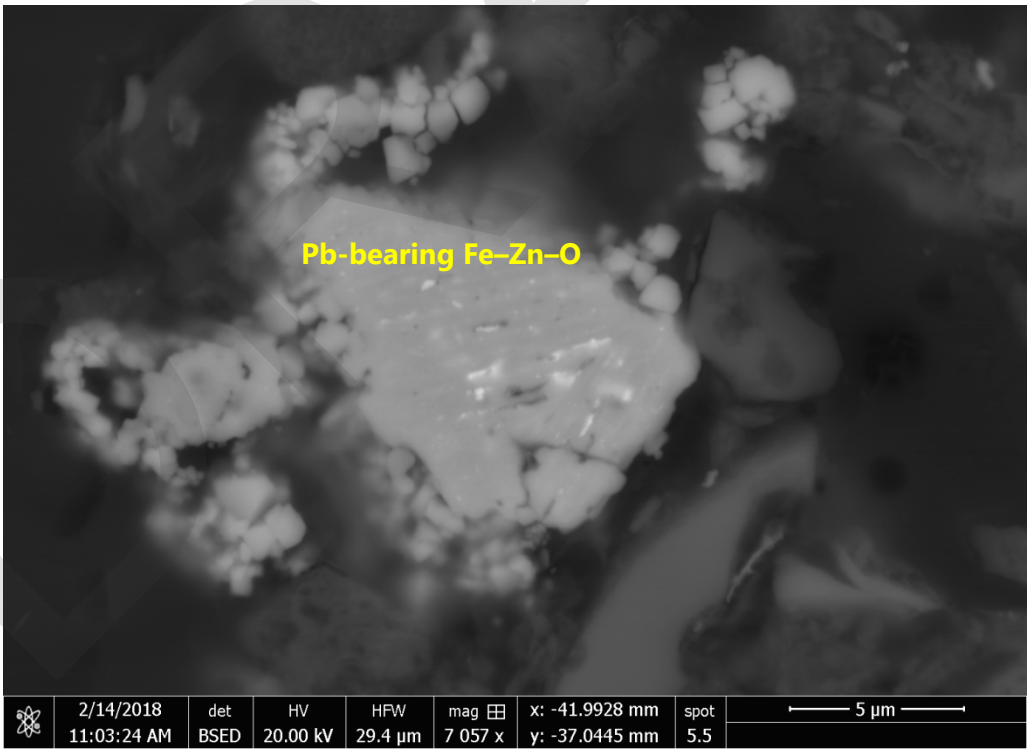

Figure I9. BSE Image of Pb-Bearing Fe–Zn–O in Sample D-401-2C, Example 1

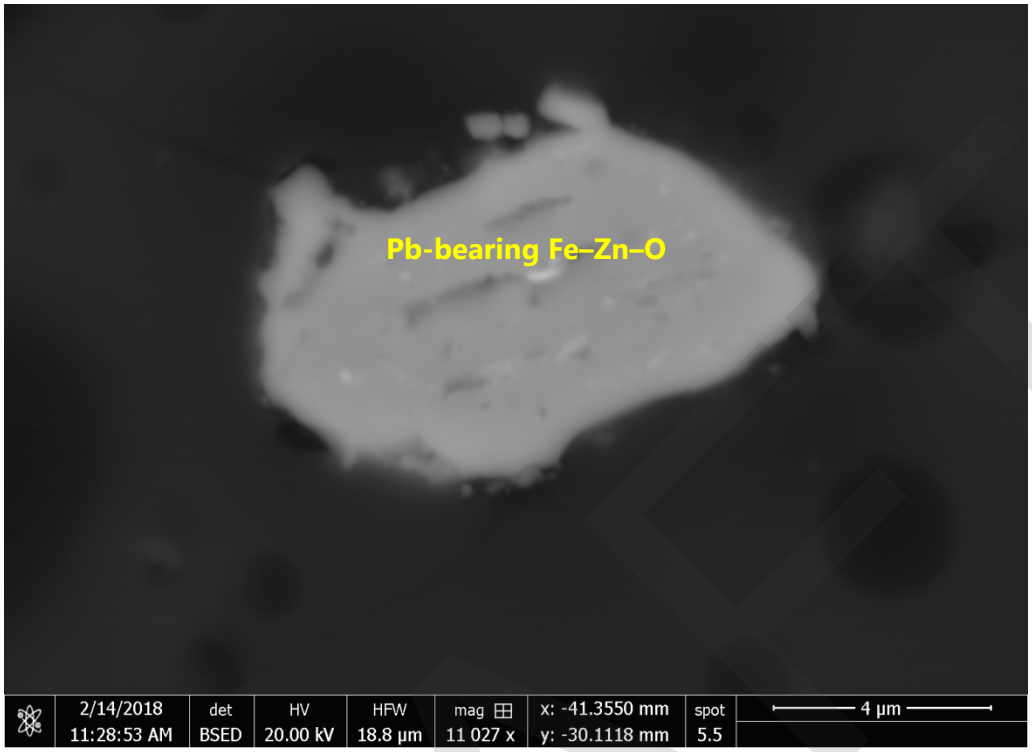

Figure I10. BSE Image of Pb-Bearing Fe–Zn–O in Sample D-401-2C, Example 2

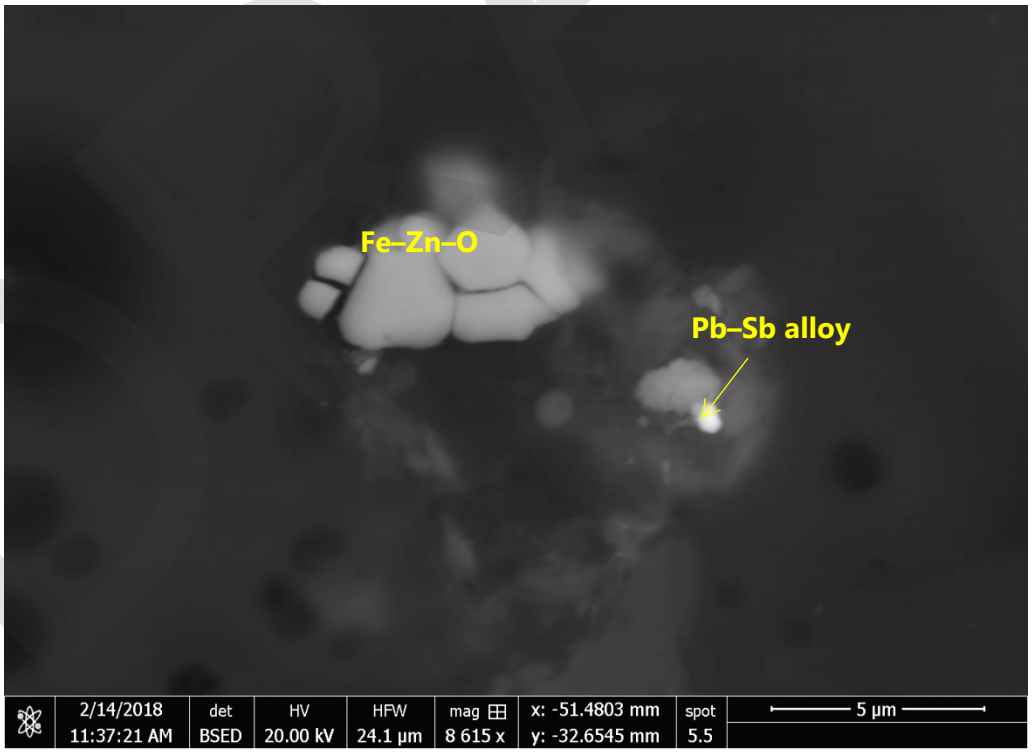

Figure I11. BSE Image of Pb–Sb-Alloy in Sample D-401-2C, Example 1

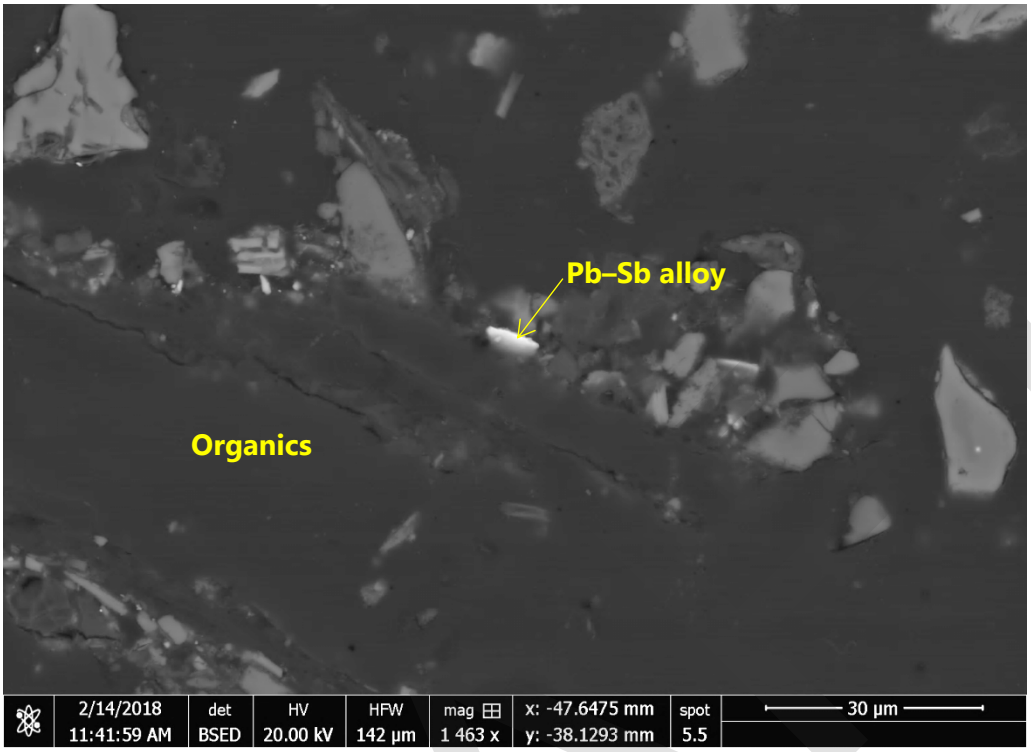

Figure I12. BSE Image of Pb–Sb-Alloy in Sample D-401-2C, Example 2

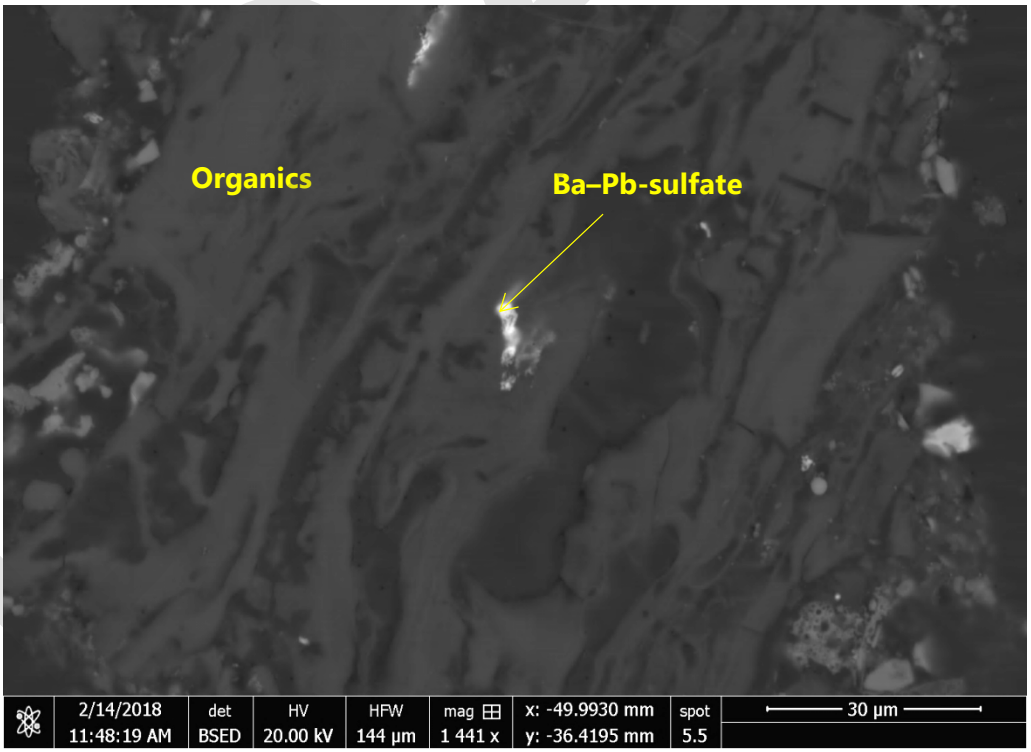

Figure I13. BSE Image of Pb–Sb-Alloy in Sample D-401-2C

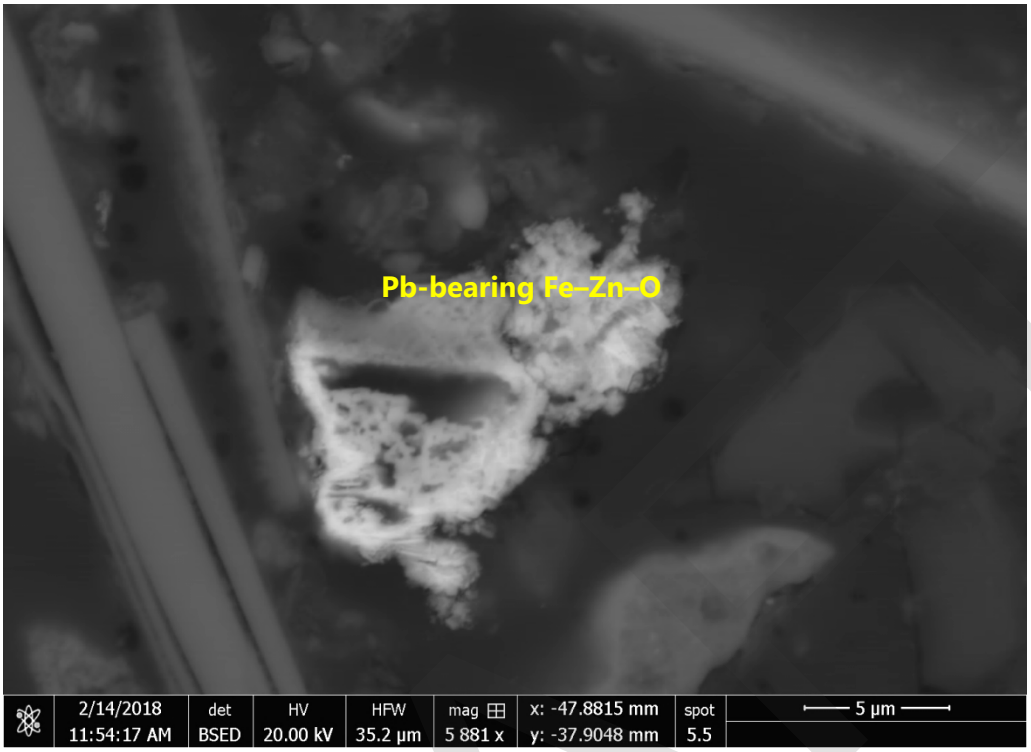

Figure I14. BSE Image of Pb-Bearing Fe–Zn–O in Sample D-401-2C, Example 3

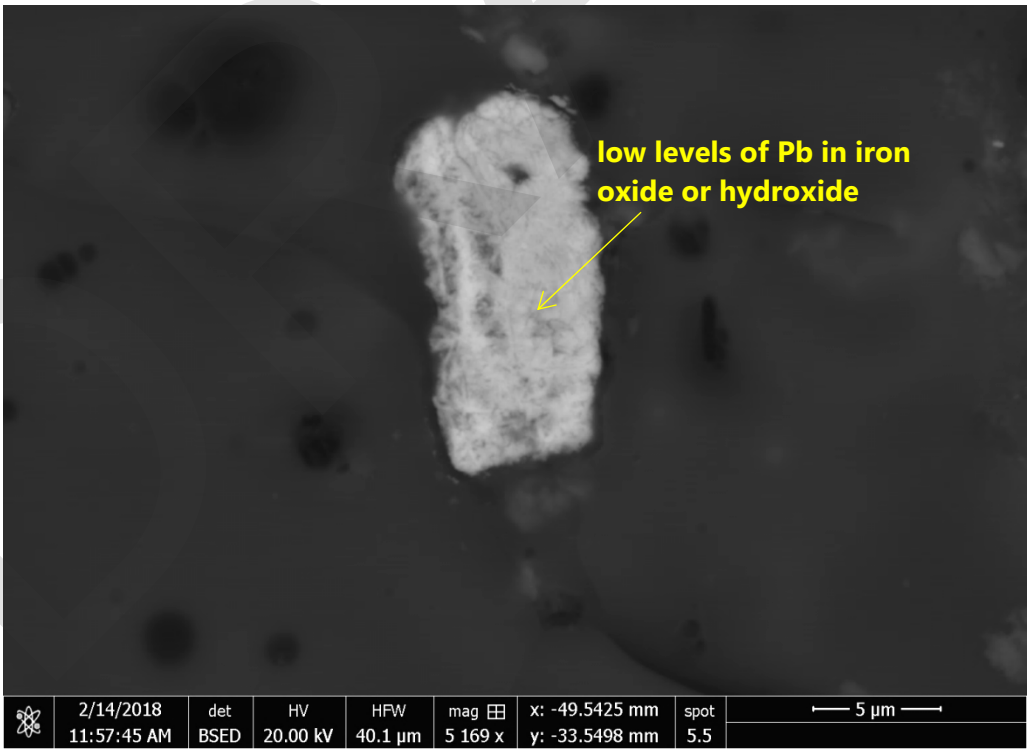

Figure I15. BSE Image of Pb-Bearing Fe-Oxide or Hydroxide in Sample D-401-2C

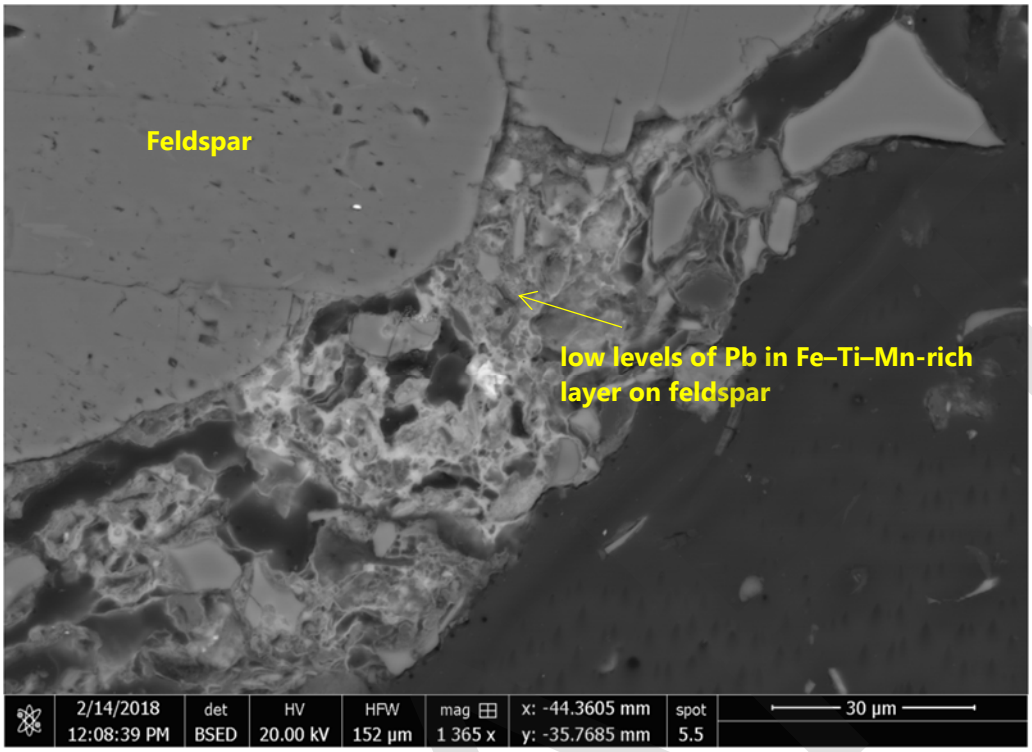

Figure I16. BSE Image of Pb-Bearing Layer on Feldspar in Sample D-401-2C

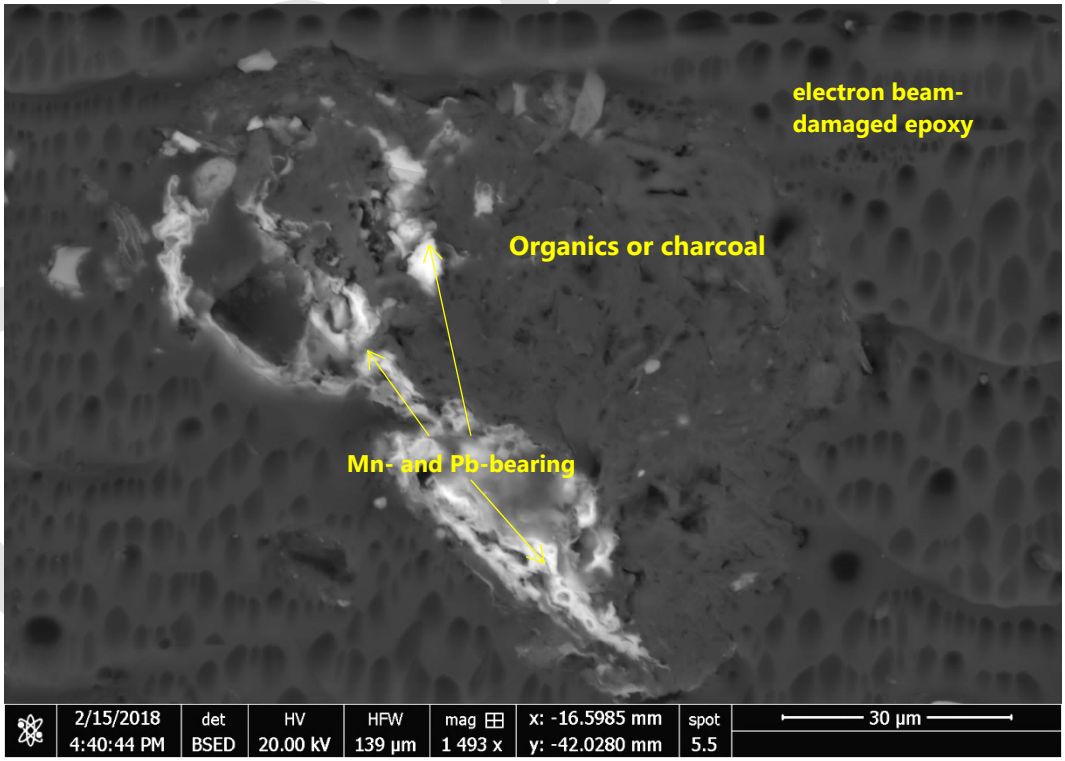

Figure I17. Mn- and Pb-Bearing Phase Associated with Organics in Sample D-258-3C

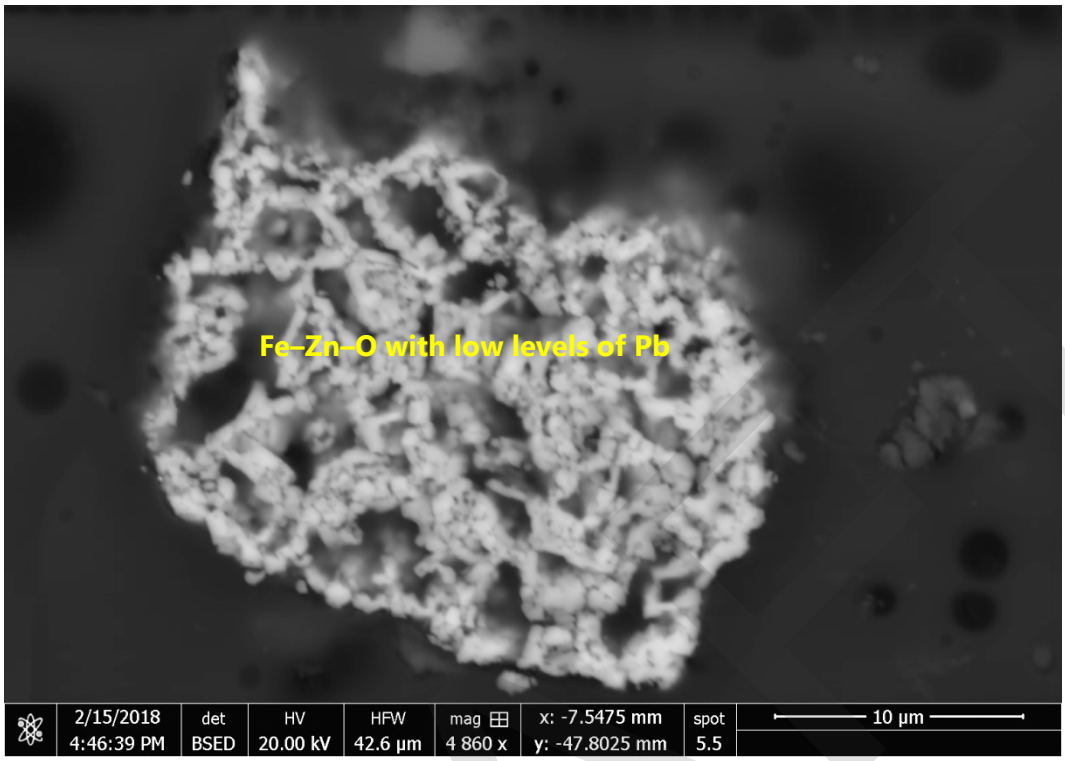

Figure I18. Pb-Bearing Fe–Zn–O in Sample D-258-3C, Example 1

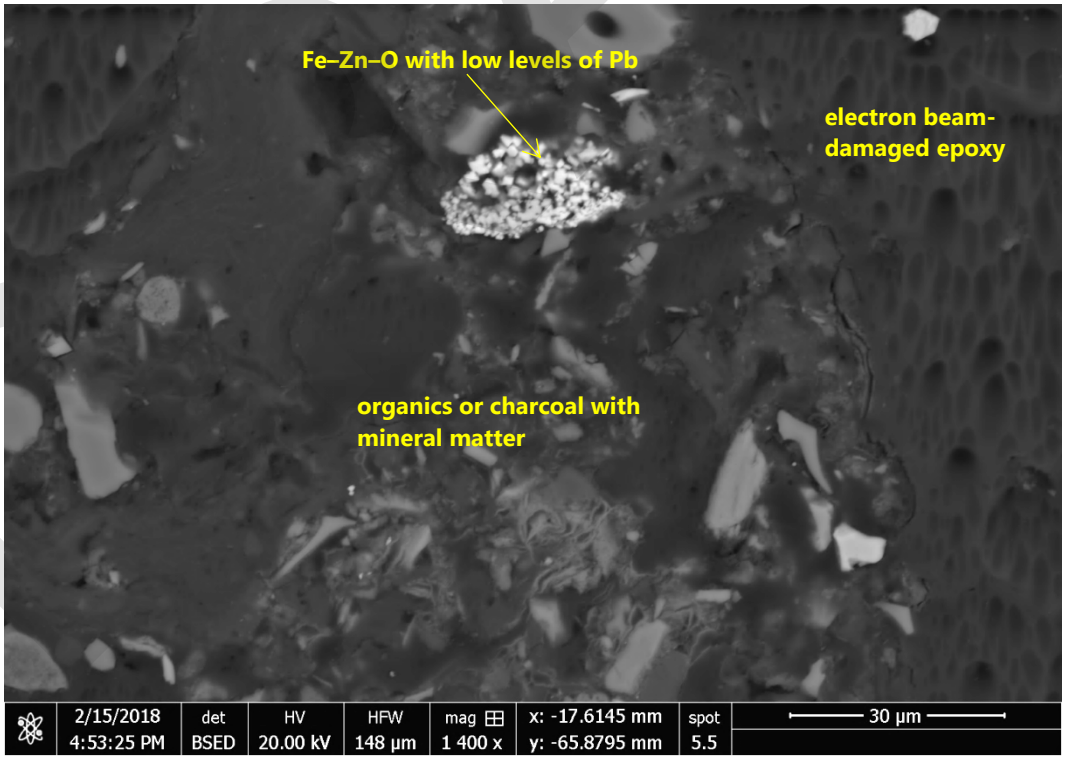

Figure I19. Pb-Bearing Fe–Zn–O in Sample D-258-3C, Example 2

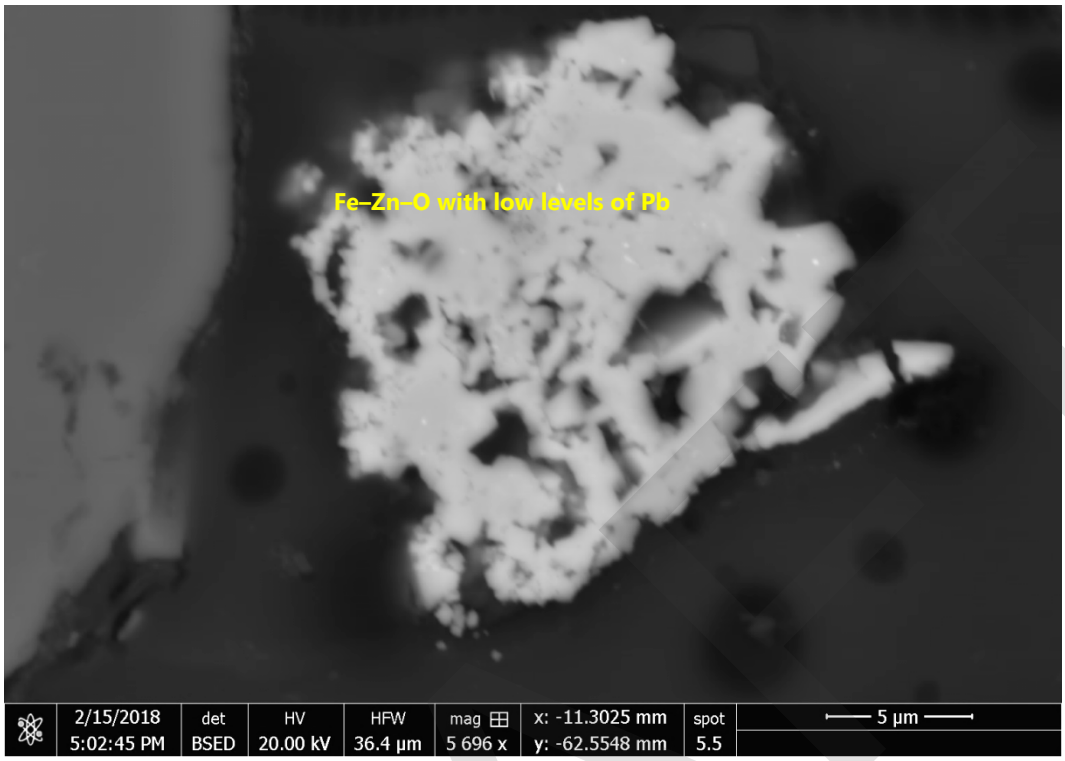

Figure I20. Pb-Bearing Fe–Zn–O in Sample D-258-3C, Example 3

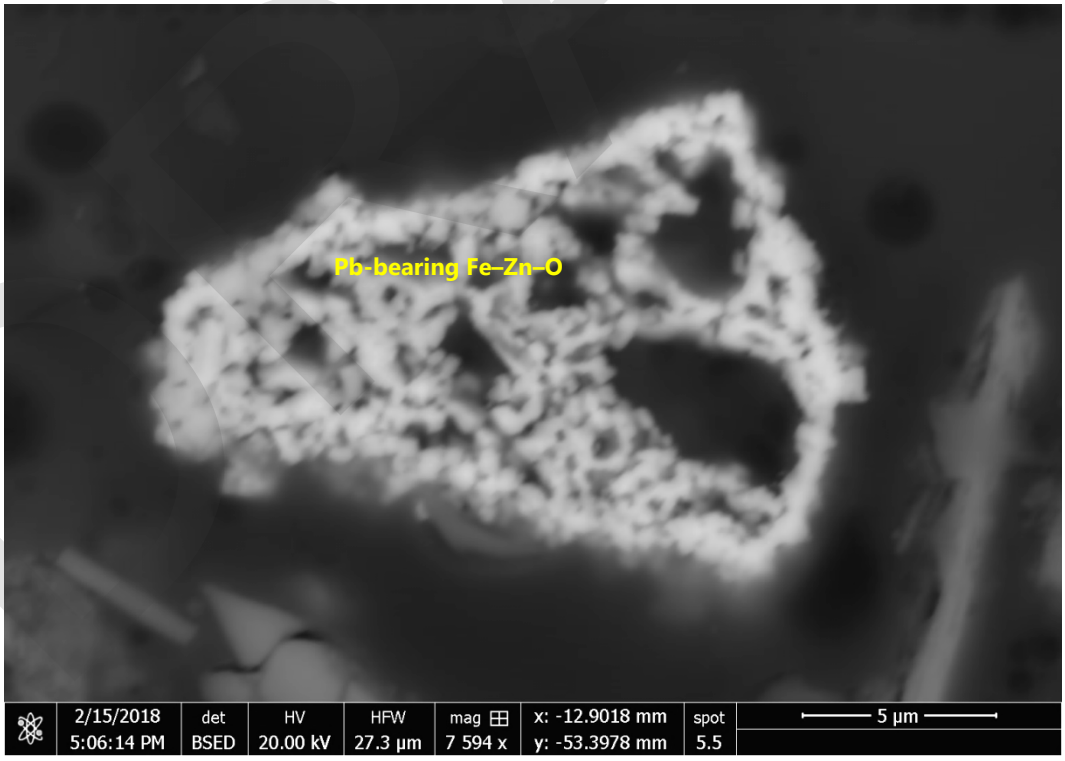

Figure I21. Pb-Bearing Fe–Zn–O in Sample D-258-3C, Example 4

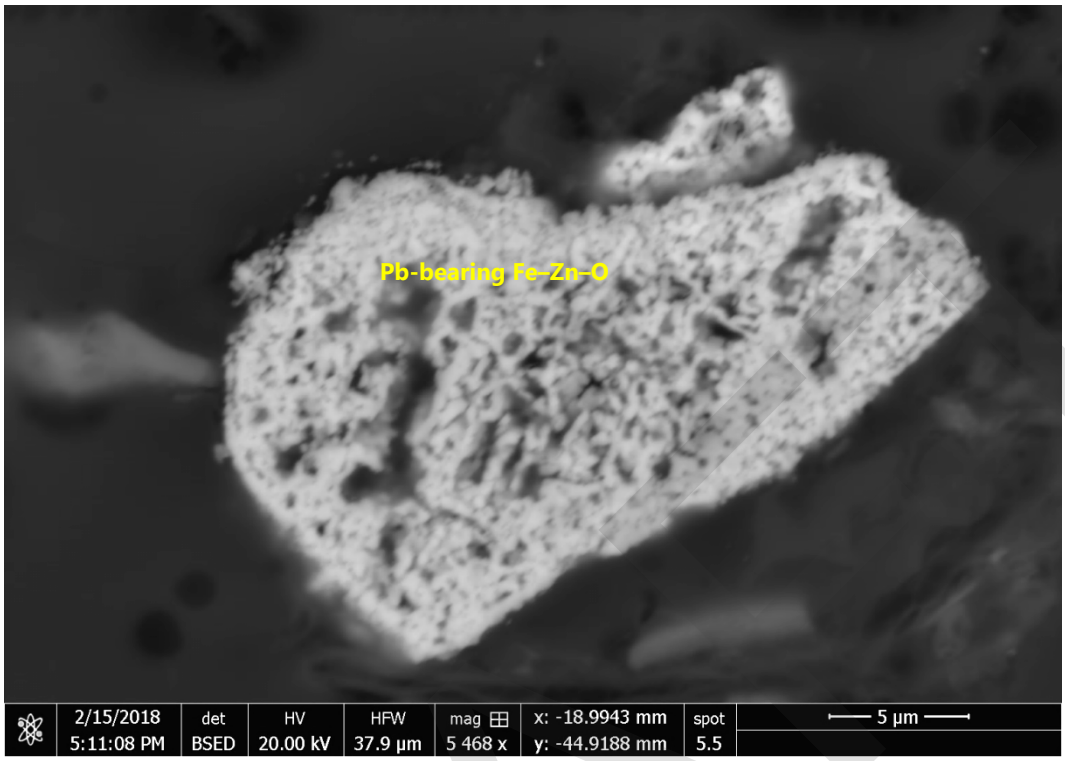

Figure I22. Pb-Bearing Fe–Zn–O in Sample D-258-3C, Example 5

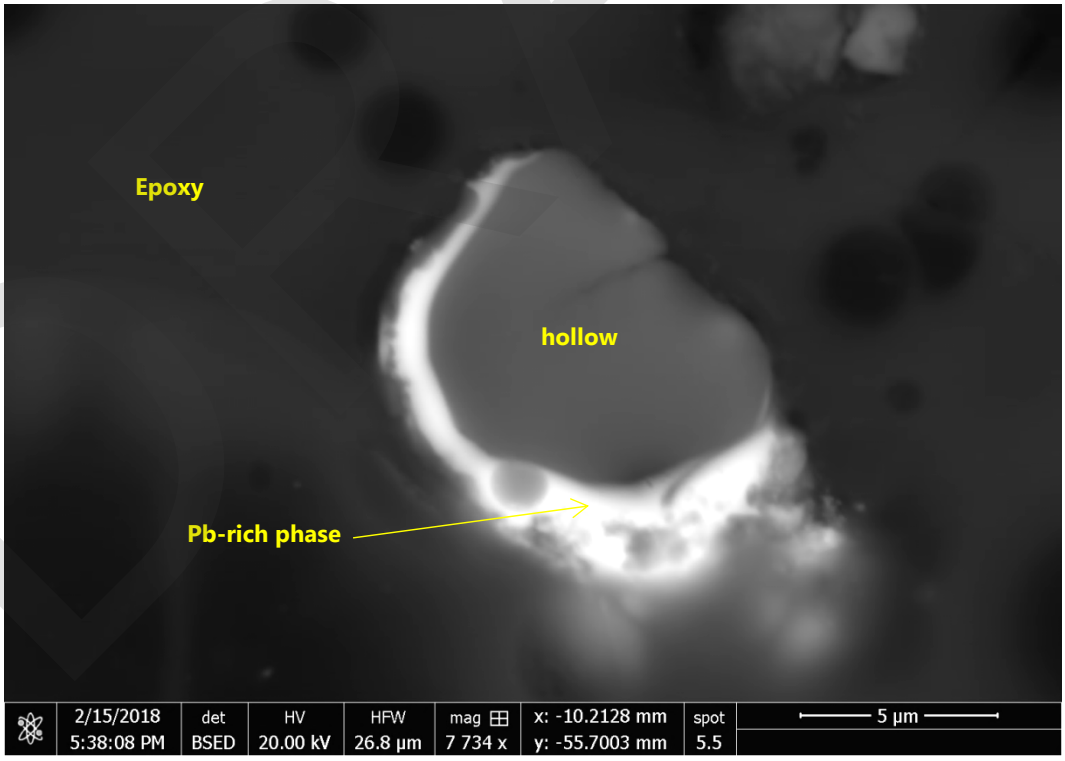

Figure I23. Unidentified Pb-Bearing Phase in Sample D-258-3C

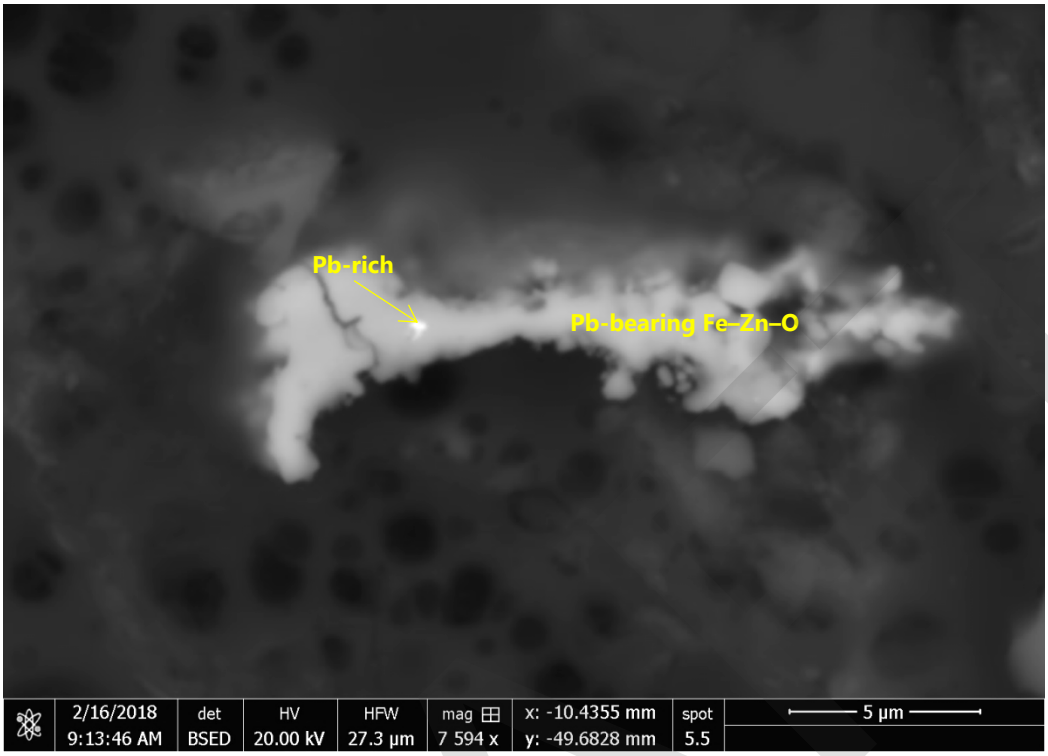

Figure I24. Pb-Bearing Fe–Zn–O in Sample D-258-3C, Example 6

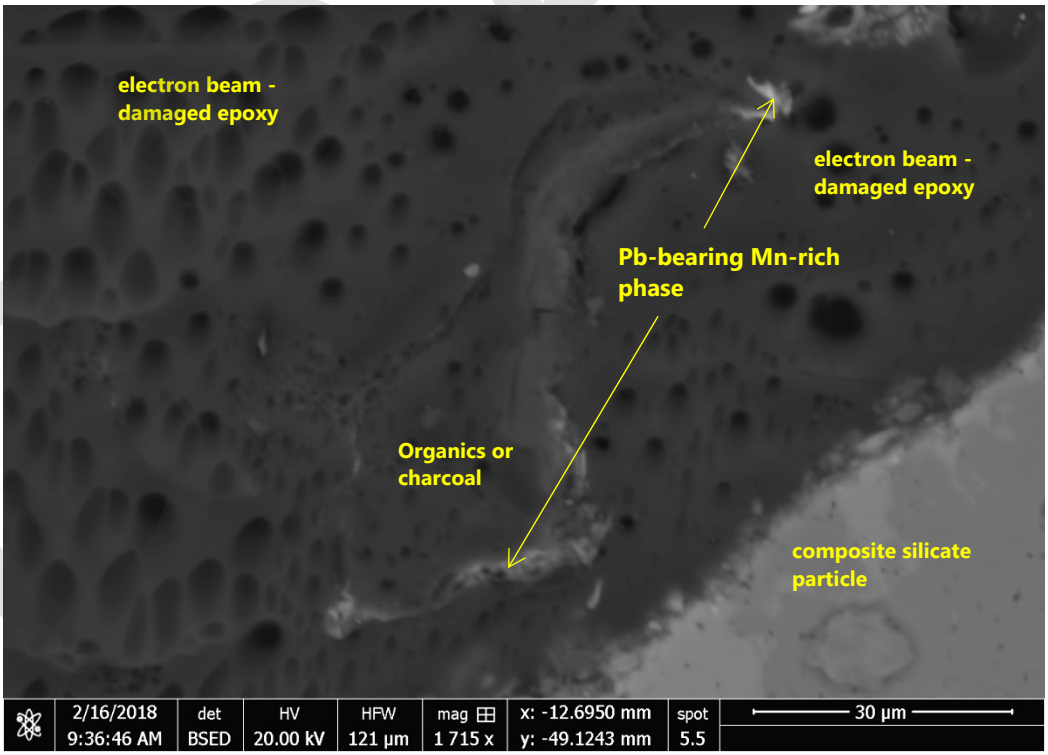

Figure I25. Pb-Bearing Mn-Rich Phase in Sample D-258-3C, Example 1

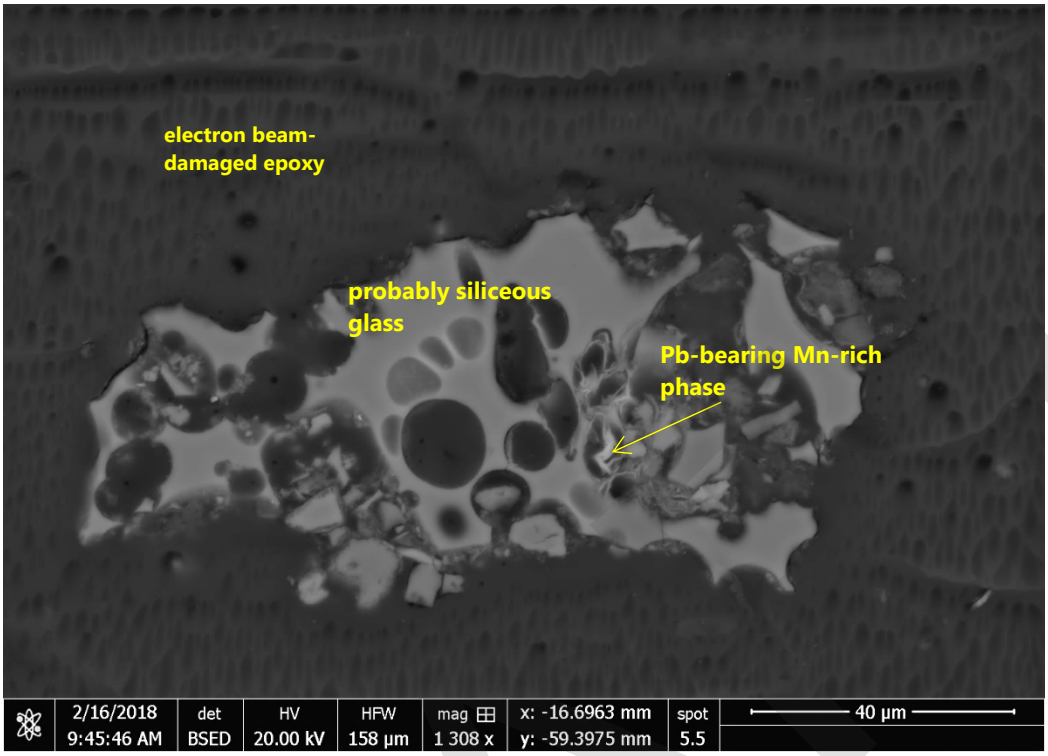

Figure I26. Pb-Bearing Mn-Rich Phase in Sample D-258-3C, Example 2

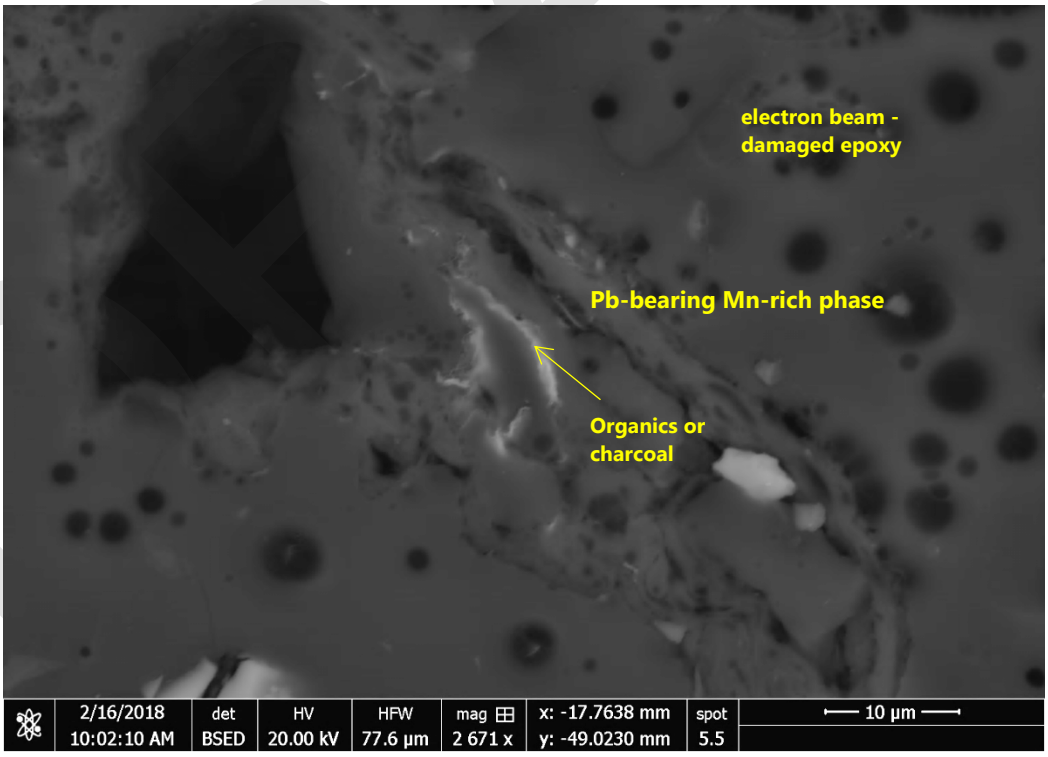

Figure I27. Pb-Bearing Mn-Rich Phase in Sample D-258-3C, Example 3

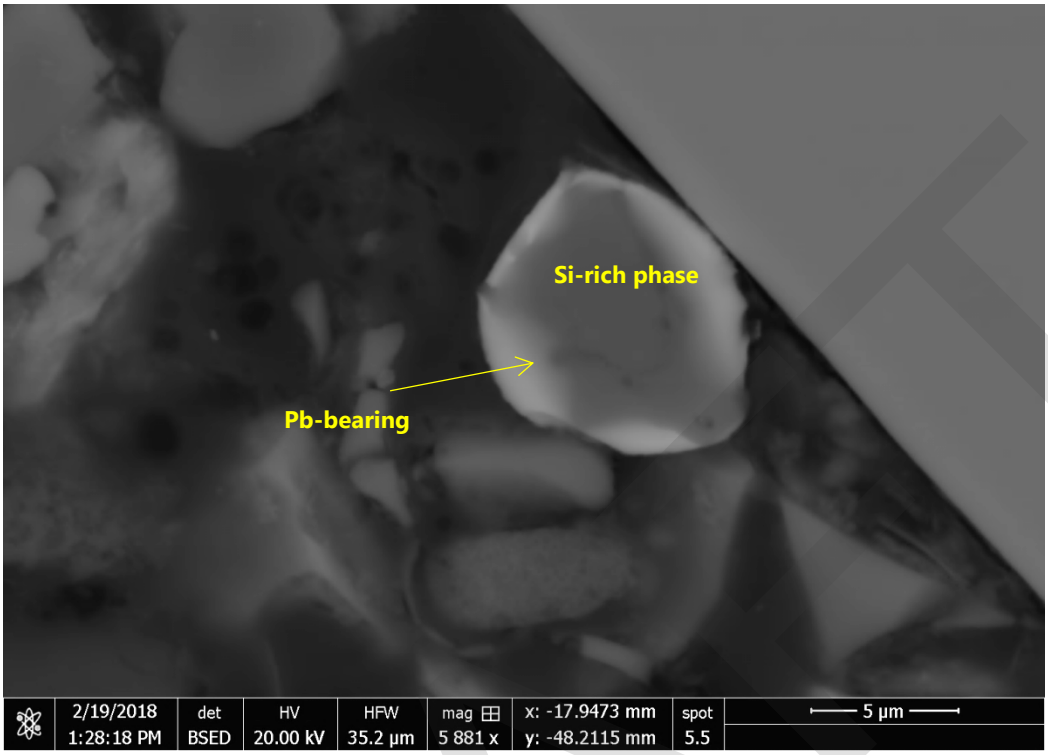

Figure I28. Pb-Bearing Rim on Siliceous Phase in Sample D-258-3C

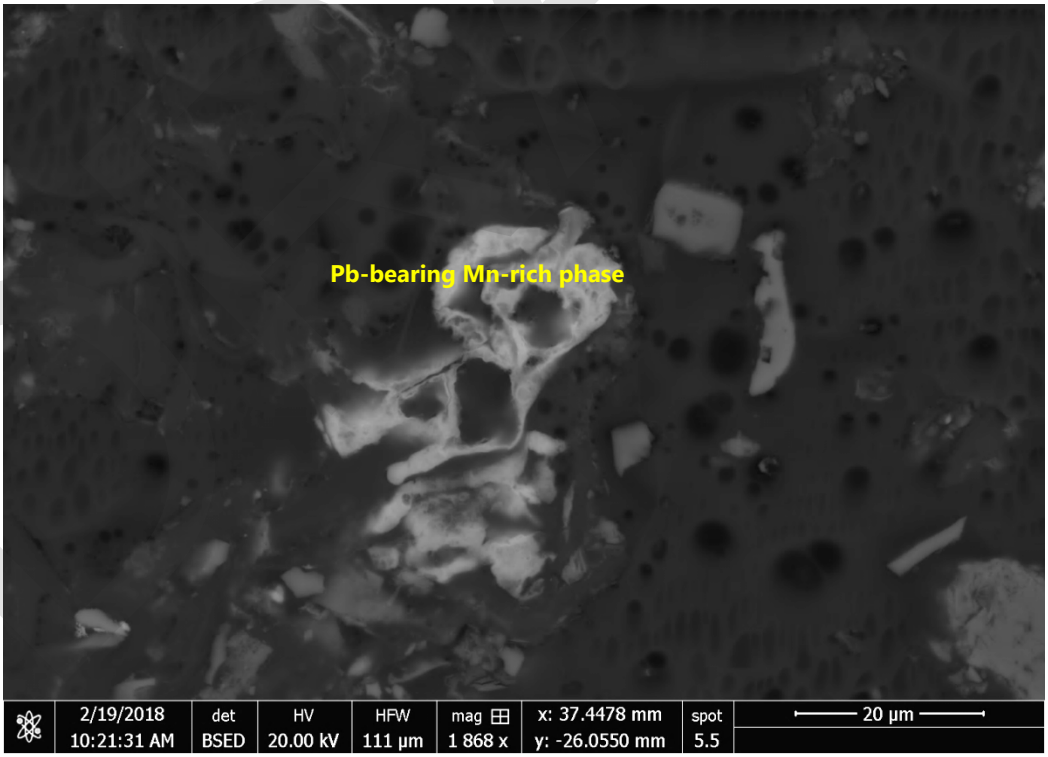

Figure I29. Pb-Bearing Mn-Rich Phase in Sample D-441-1B, Example 1

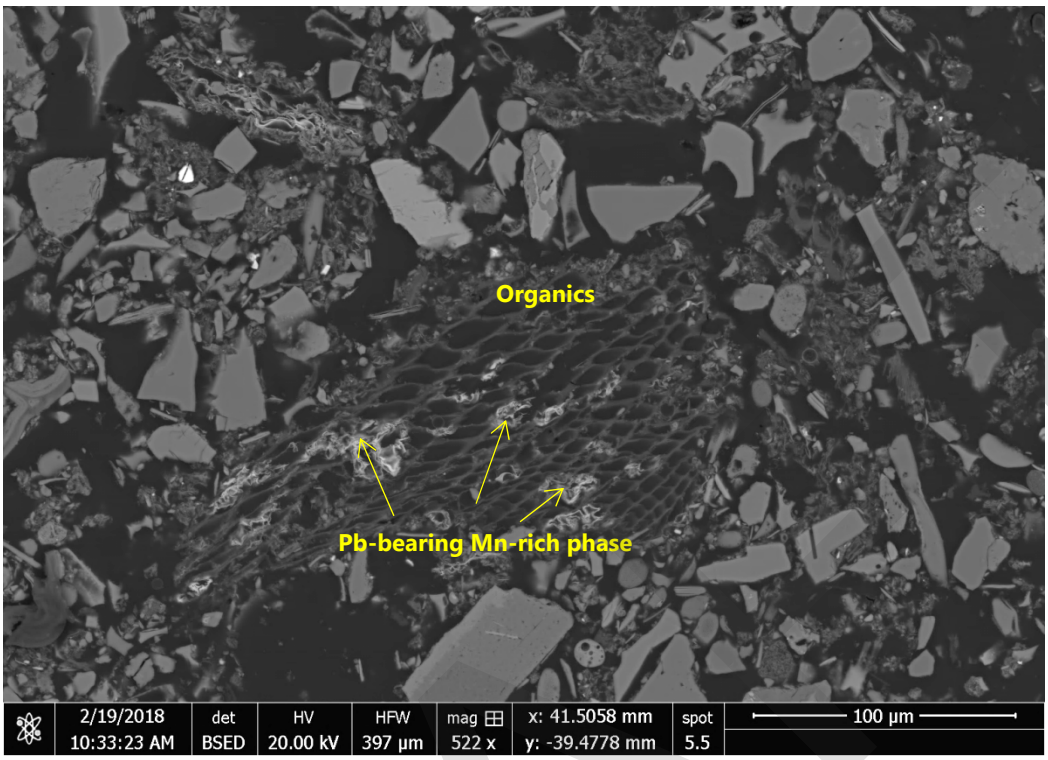

Figure I30. Pb-Bearing Mn-Rich Phase Associated with Organics in Sample D-441-1B

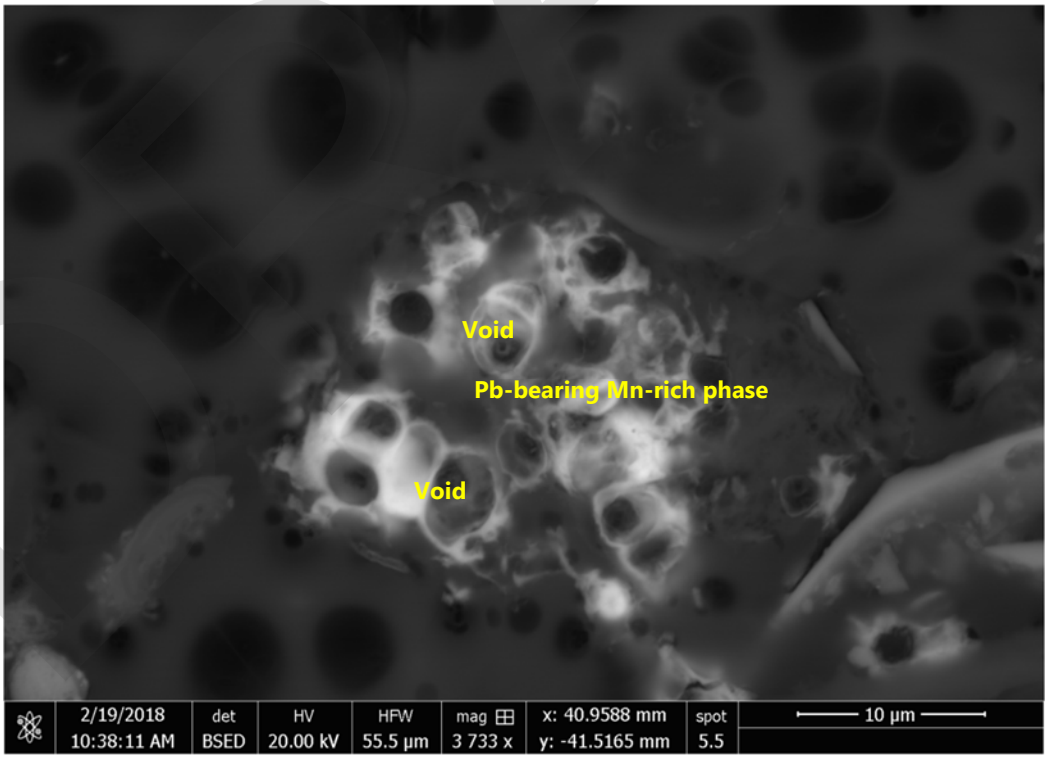

Figure I31. Pb-Bearing Mn-Rich Phase in Sample D-441-1B, Example 2

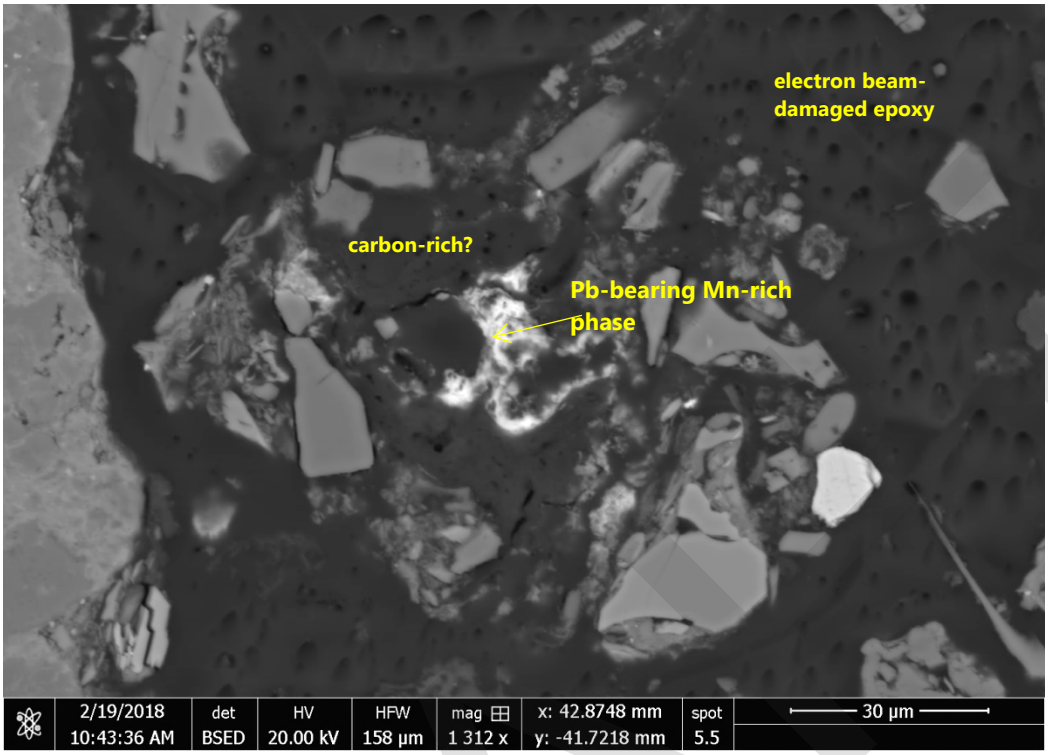

Figure I32. Pb-Bearing Mn-Rich Phase in Sample D-441-1B, Example 3

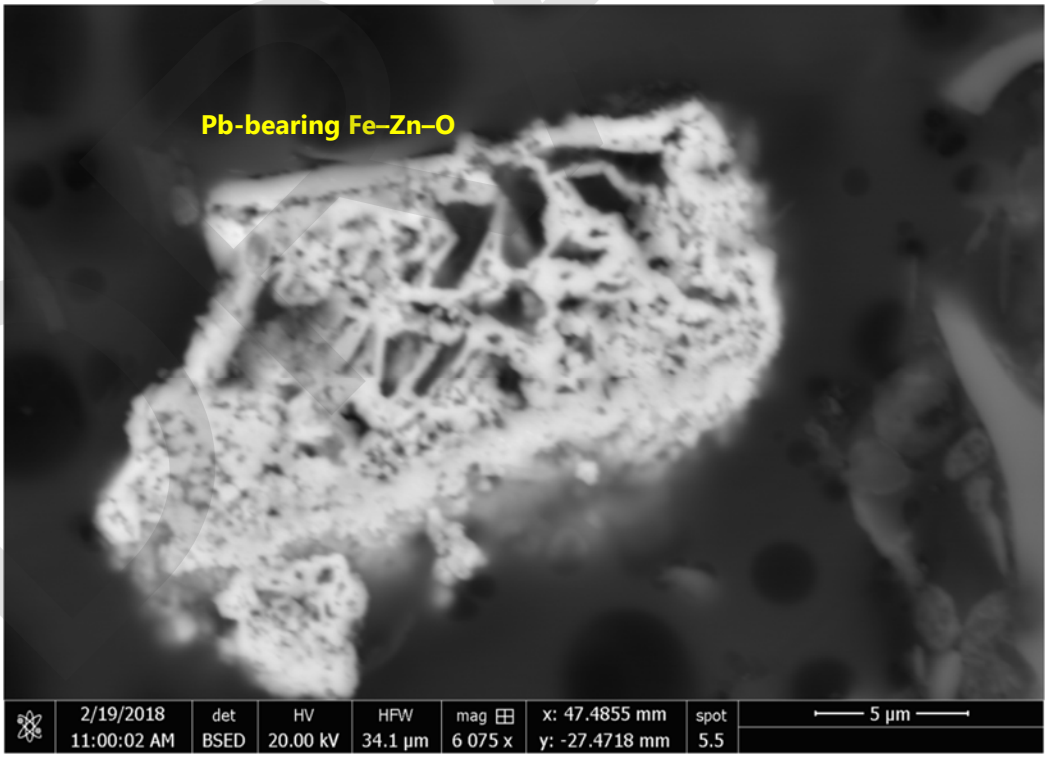

Figure I33. Pb-Bearing Fe–Zn–O Phase in Sample D-441-1B

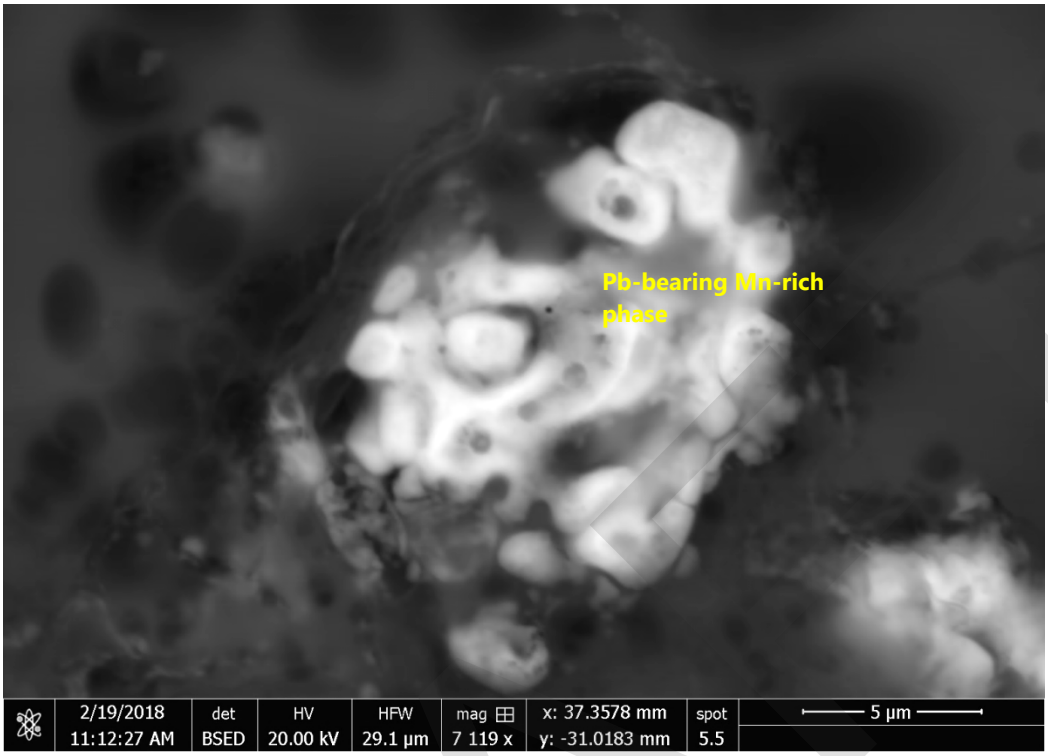

Figure I34. Pb-Bearing Mn-Rich Phase in Sample D-441-1B, Example 4

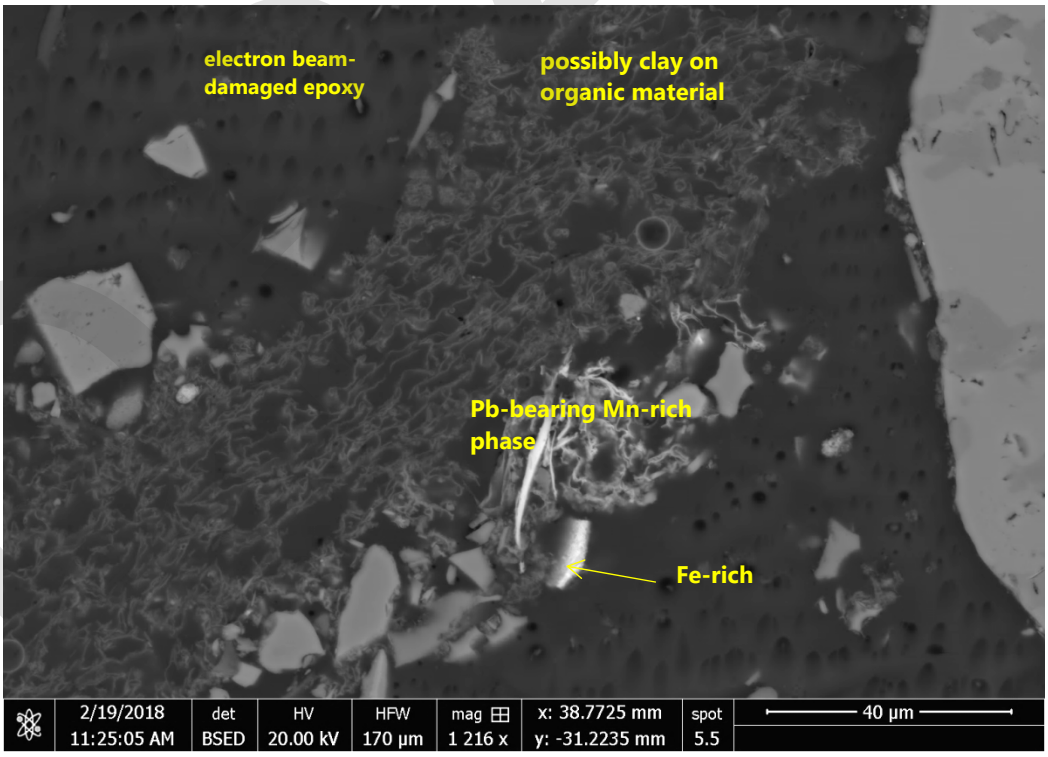

Figure I35. Pb-Bearing Mn-Rich Phase in Sample D-441-1B, Example 5

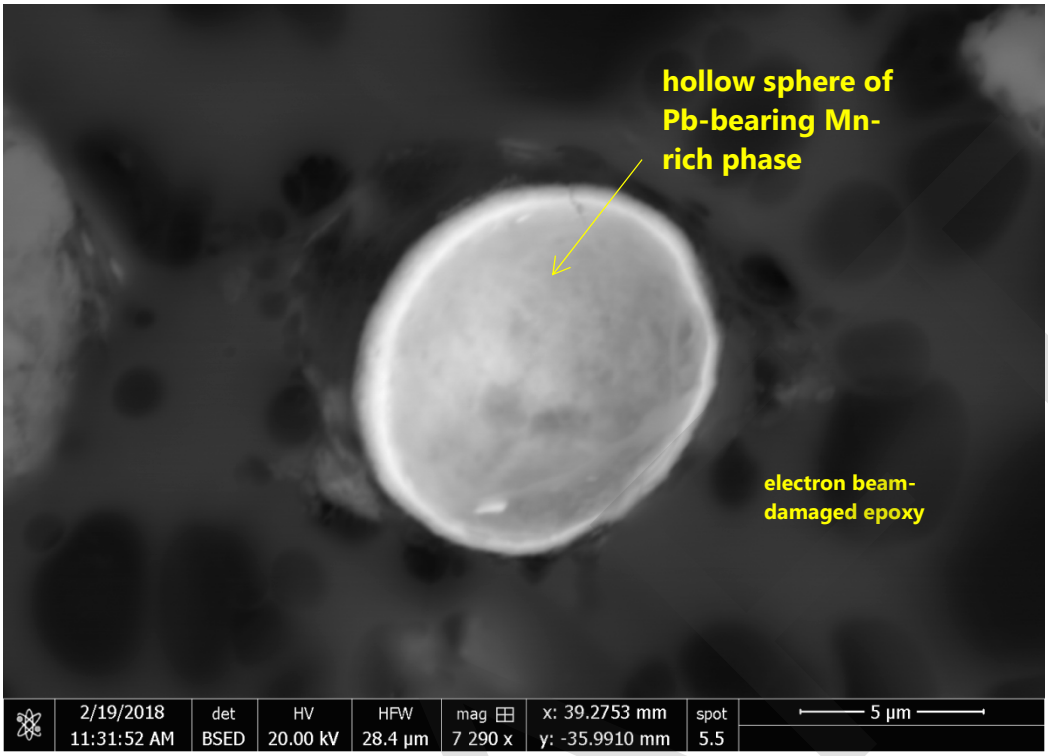

Figure I36. Pb-Bearing Mn-Rich Hollow Sphere in Sample D-441-1B

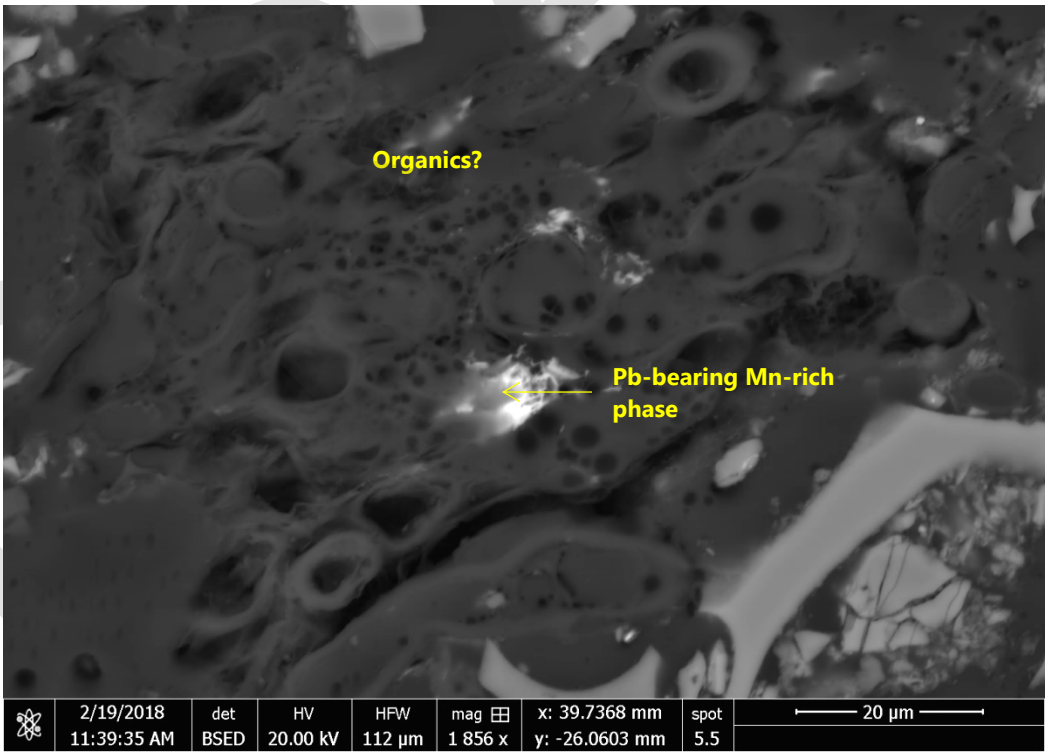

Figure I37. Pb-Bearing Mn-Rich Phase in Sample D-441-1B, Example 6

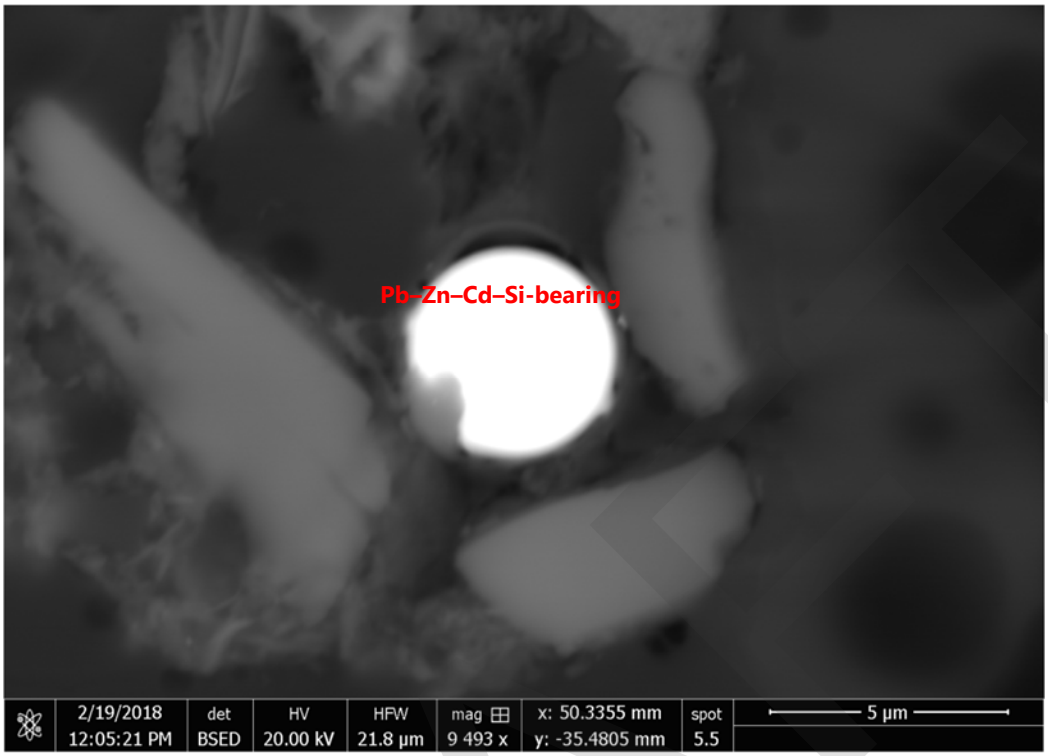

Figure I38. Spherical Pb–Zn–Cd–Si-Bearing Phase in Sample D-441-1B

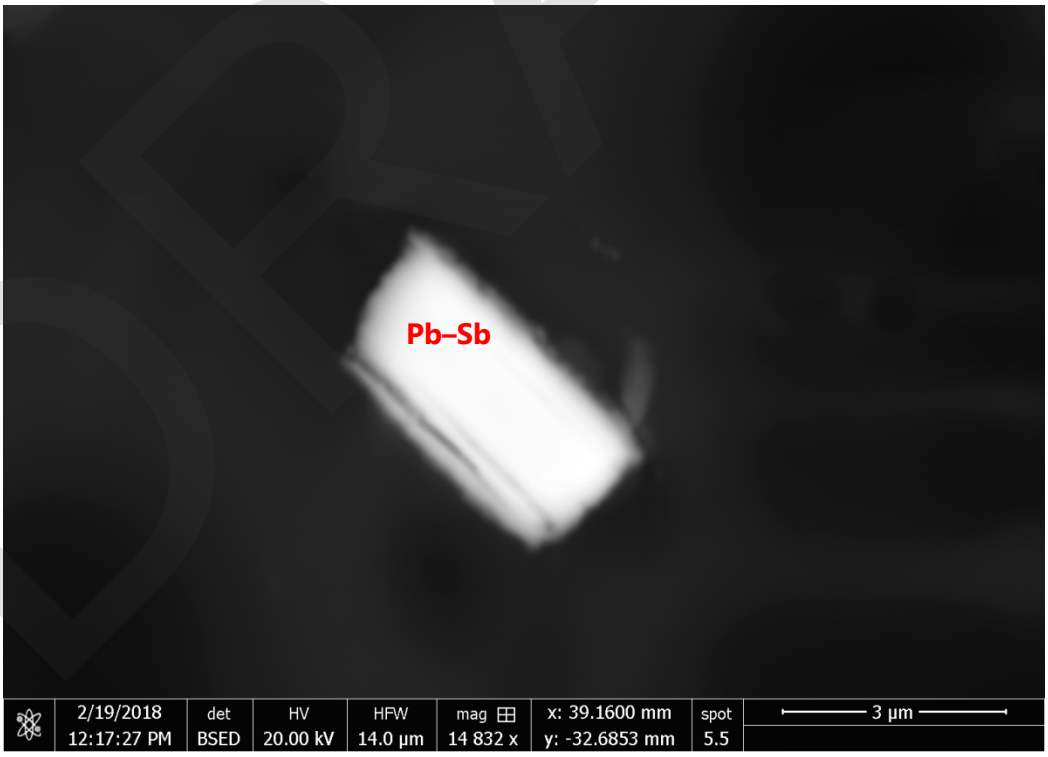

Figure I39. Pb-Sb Alloy in Sample D-441-1B, Example 1

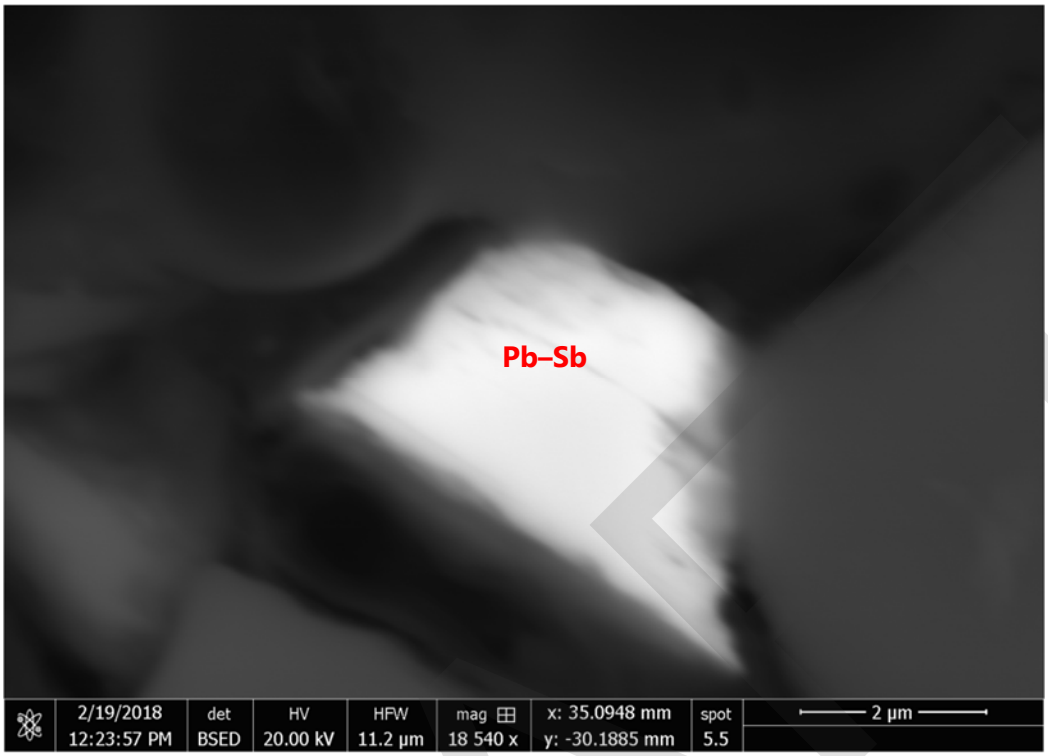

Figure I40. Pb-Sb Alloy in Sample D-441-1B, Example 2

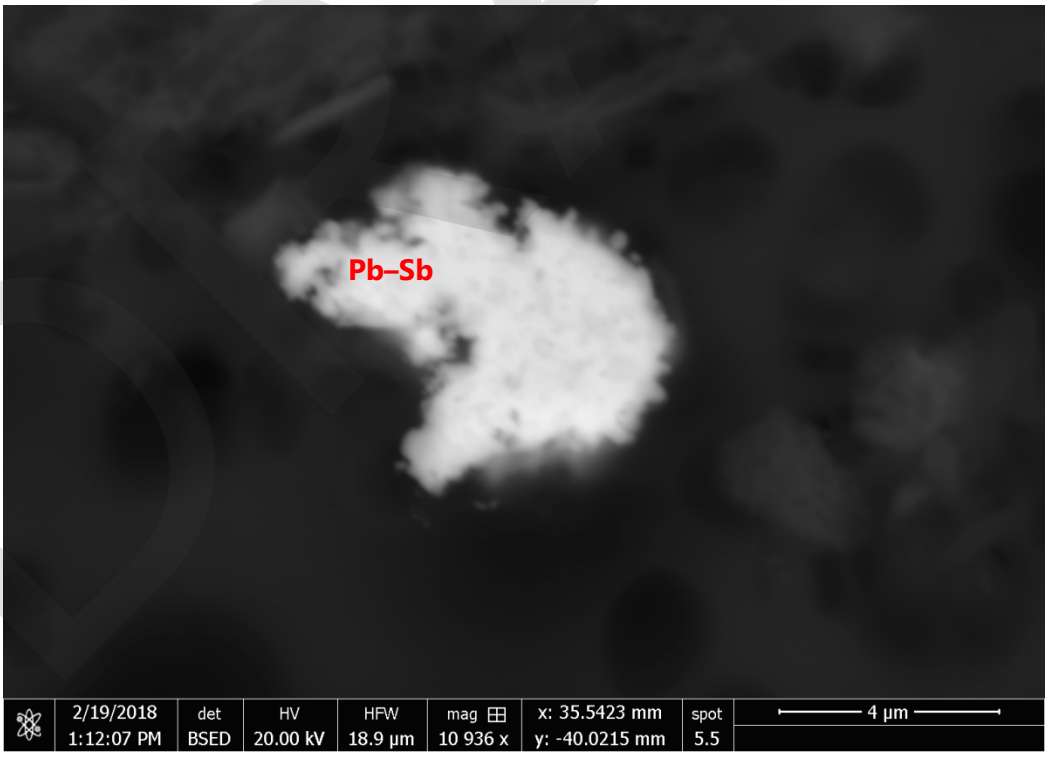

Figure I41. Pb-Sb Alloy in Sample D-441-1B, Example 3